Light-quark $SU(3)$ flavor splitting of heavy-light constituent diquark masses and doubly strange diquarks from QCD sum rules

T. de Oliveira[,1,*] D. Harnett[,1,†] R. Kleiv[,2,‡] A. Palameta[,3,§] and T. G. Steele[,1,‖]

[1]*Department of Physics & Engineering Physics, University of Saskatchewan,*
Saskatoon, Saskatchewan S7N 5E2, Canada
[2]*Department of Physical Sciences (Physics), Thompson Rivers University,*
Kamloops, British Columbia V2C 0C8, Canada
[3]*Department of Physics, University of the Fraser Valley, Abbotsford, British Columbia V2S 7M8, Canada*

QCD Laplace sum rules are used to examine the constituent mass spectrum of $J^P \in \{0^+, 1^+\}$ (scalar, axial vector) heavy-light $[Qq]$ diquarks with $Q \in \{c, b\}$ (charm, bottom) and $q \in \{u, d, s\}$ (up, down, strange). As in previous sum-rule studies, the negative parity $J^P \in \{0^-, 1^-\}$ (pseudoscalar, vector) $[Qq]$ diquark mass predictions do not stabilize, so the sum-rule analysis focuses on positive parity $[Qq]$ diquarks. Doubly strange $J^P = 1^+$ (axial vector) $[ss]$ diquarks are also examined, but the resulting sum rules do not stabilize. Hence there is no sum-rule evidence for $J^P = 1^+$ $[ss]$ diquark states, aiding the interpretation of sum-rule analyses of fully strange tetraquark states. The $SU(3)$ flavor splitting effects for $[Qq]$ diquarks are obtained by calculating QCD correlation functions of $J^P \in \{0^+, 1^+\}$ diquark composite operators up to next-to-leading order in perturbation theory, leading-order in the strange quark mass, and in the chiral limit for nonstrange (u, d) quarks with an isospin-symmetric vacuum $\langle \bar{n}n \rangle = \langle \bar{u}u \rangle = \langle \bar{d}d \rangle$. Apart from the strange quark mass parameter m_s, the strange quark condensate parameter $\kappa = \langle \bar{s}s \rangle / \langle \bar{n}n \rangle$ has an important impact on $SU(3)$ flavor splittings. A Laplace sum-rule analysis methodology is developed for the mass difference $M_{[Qs]} - M_{[Qn]}$ between the strange and nonstrange heavy-light diquarks to reduce the theoretical uncertainties from all other QCD input parameters. The mass splitting is found to decrease with increasing κ, providing an upper bound on κ where the $M_{[Qs]} - M_{[Qn]}$ mass hierarchy reverses. In the typical QCD sum-rule range $0.56 < \kappa < 0.74$, $55 \text{ MeV} \lesssim M_{[cs]} - M_{[cn]} \lesssim 100 \text{ MeV}$ and $75 \text{ MeV} \lesssim M_{[bs]} - M_{[bn]} \lesssim 150 \text{ MeV}$, with a slight tendency for larger splittings for the $J^P = 1^+$ axial-vector channels. These constituent mass splitting results are discussed in comparison with values used in constituent diquark models for tetraquark and pentaquark hadronic states.

I. INTRODUCTION

Over the past two decades, numerous mesons have been discovered that do not fit within the conventional quark model of quark-antiquark states (see e.g., Refs. [1–9] for reviews). Exotic four-quark meson configurations anticipated long ago [10,11] seem to be realized in nature with astounding richness and complexity. Noteworthy recent discoveries of four-quark states include the doubly charged open-charm state $T^a_{c\bar{s}0}(2900)^{++}$ (and its neutral partner) [12,13]; the fully closed charm $X(6900)$ [$T_{\psi\psi}(6900)$ in the Ref. [14] naming scheme] [15]; open-charm states $X_0(2900)$ and $X_1(2900)$ [$T_{cs0}(2900)^0$ and $T_{cs1}(2900)^0$] [16,17]; and the hidden-charm states $Z_{cs}(3985)^-$, $Z_{cs}(4000)^+$, $Z_{cs}(4220)^+$ [18,19].

An important scenario for four-quark mesons is the compact tetraquark scenario involving the interaction of colored diquark-antidiquark constituents [20,21]. Various models can then be used to determine tetraquark properties in this diquark-antidiquark scenario, including types I and II diquark models [22–27], dynamical quark model [28], relativized diquark model [29–33], relativistic quark model [34–38], and the diquark effective Hamiltonian model [39]. The constituent diquark masses are one of the crucial input parameters in these models, and depending on the model, the diquark constituent mass is either fit to

*tdo842@usask.ca
†derek.harnett@shaw.ca
‡rkleiv@tru.ca
§alexander.palameta@ufv.ca
‖tom.steele@usask.ca

the observed tetraquark candidates or is separately determined (or estimated) within the model itself. Diquark constituent masses are also important ingredients in various pentaquark models (see, e.g., [40–42]).

Because of the crucial role of the diquark constituent mass in tetraquark (and pentaquark) models, it is important to determine whether there is supporting QCD evidence for the diquark constituent mass parameters used in these models. QCD sum rules [43,44] (see, e.g., [45–48] for reviews) have been used to predict diquark constituent masses for various J^P combinations for light-light diquarks [49–51], heavy-light diquarks [52–54], and doubly heavy diquarks [55]. Overall, these QCD sum-rule diquark constituent mass predictions are in good agreement with the values used in the various diquark models, providing QCD evidence supporting the tetraquark and pentaquark mass predictions emerging from these models. For example, in Ref. [55], $[cc]$ and $[bb]$ axial vector constituent diquark masses were calculated using QCD sum rules and results were compared with different diquark models of fully heavy $[cc][\bar{c}\,\bar{c}]$ and $[bb][\bar{b}\,\bar{b}]$ tetraquark states.

One of the challenges of QCD sum-rule methods is determining the light flavor hadronic mass splittings because theoretical uncertainties tend to obscure the small differences between systems with strange quarks and those with non-strange quarks. For example, approaches that separately predict hadronic masses in strange and nonstrange systems typically result in masses that overlap in the bands of theoretical uncertainty, preventing reliable determination of light-flavor mass splittings. Examples relevant to exotic hadron systems include Refs. [54,56–60]. However, QCD sum-rule analysis methods such as double-ratios predict the light-flavor splittings and provide better control over theoretical uncertainties [61].

In this paper, QCD Laplace sum rules are used to calculate the constituent mass spectrum of $J^P \in \{0^+, 1^+\}$ (scalar, axial vector) heavy-light $[Qq]$ diquarks with $Q \in \{c, b\}$ (charm, bottom), and $q \in \{u, d, s\}$ (up, down, strange). Doubly strange $[ss]$ $J^P = 1^+$ diquarks are also considered, extending the Ref. [55] sum-rule analysis of $[cc]$ and $[bb]$ diquarks to the strange sector.[1] Our methodology begins with a baseline prediction of the nonstrange constituent masses $M_{[Qn]}$ (updating Ref. [52] to reflect improved determinations of quark mass parameters). In this baseline analysis it is found that negative parity $J^P \in \{0^-, 1^-\}$ mass predictions do not stabilize as in Ref. [52], nor do those of $J^P = 1^+$ $[ss]$ diquarks. Further analysis of $[Qq]$ diquarks therefore focuses on the $J^P \in \{0^+, 1^+\}$ diquarks. From this baseline, the double-ratio method [61] is extended to predict the flavor-splitting mass difference $M_{[Qs]} - M_{[Qn]}$ between strange and nonstrange heavy-light diquarks. This analysis builds upon Ref. [54] in two

significant ways by including next-to-leading order (NLO) perturbative effects, and reducing the theoretical uncertainty in $M_{[Qs]} - M_{[Qn]}$ through our mass-splitting methodology.

As shown below, the strange quark condensate parameter $\kappa = \langle \bar{s}s \rangle / \langle \bar{n}n \rangle$, (i.e., $\langle \bar{n}n \rangle = \langle \bar{u}u \rangle = \langle \bar{d}d \rangle$) has an important impact on $SU(3)$ flavor splittings. The mass splitting is found to decrease with increasing κ, providing an upper bound on κ where the $M_{[Qs]} - M_{[Qn]}$ mass hierarchy reverses. In the typical QCD sum-rule range for κ, the constituent mass splitting predictions are discussed in comparison with values used in constituent diquark models for tetraquark and pentaquark states.

II. DIQUARK CORRELATION FUNCTIONS

QCD sum rules use correlation functions of composite operators to probe the properties of bound states corresponding to the valence content of the operator [43,44] (see, e.g., [45–48] for reviews). The dispersion relation satisfied by the correlation function then establishes a duality relation between the QCD prediction and a spectral function for the bound states. Families of sum rules are then constructed by transforming the dispersion relation (e.g., the Borel [43,44] transform used to obtain Laplace sum rules).

The correlation function for heavy-light diquark systems is defined as

$$\Pi^{(\Gamma)}(Q^2) = i \int d^D x e^{iq \cdot x} \langle \Omega | T[J_\alpha^{(\Gamma)}(x) S_{\alpha\omega}(x,0) J_\omega^{(\Gamma)\dagger}(0)] | \Omega \rangle,$$

(1)

where $Q^2 = -q^2$, $\{\alpha, \omega\}$ are color indices, $D = 4 + 2\epsilon$ is the spacetime dimension for dimensional regularization, $S_{\alpha\omega}(x,0)$ is the Schwinger string [see Eq. (6)], and $J_\alpha^{(\Gamma)}(x)$ represents the heavy-light color-triplet diquark currents [49,50]

$$J_\alpha^{(\Gamma)}(x) = \epsilon_{\alpha\beta\gamma} Q_\beta^T(x) C \mathcal{O}_\Gamma q_\gamma(x)$$

(2)

with $\epsilon_{\alpha\beta\gamma}$ a Levi-Civita symbol in quark color space, Q denoting a heavy-quark (charm c or bottom b), and q representing a light-quark (either strange s or nonstrange $n \in \{u, d\}$), T is the transpose, and C is the charge conjugation operator. In Eq. (2), the operator $\mathcal{O}_\Gamma$

$$\mathcal{O}_\Gamma \in \{I, \gamma_5, \gamma_\mu, \gamma_\mu \gamma_5\},$$

(3)

respectively, probes the pseudoscalar ($\Gamma = P$, $J^P = 0^-$), scalar ($\Gamma = S$, $J^P = 0^+$), axial vector ($\Gamma = A$, $J^P = 1^+$), and vector ($\Gamma = V$, $J^P = 1^-$) diquark states. The axial-vector and vector diquark states are extracted from projections of (1)

$$\Pi^{(A,V)}(Q^2) = \frac{1}{D-1} \left(\frac{q^\mu q^\nu}{q^2} - g^{\mu\nu} \right) \Pi_{\mu\nu}^{(A,V)}(q),$$

(4)

---

[1]The $[Qq]$ and $[ss]$ notation is used only to denote the diquark flavor content and not the flavor symmetry properties.

while for the scalar and pseudoscalar cases Π^S and Π^P are used directly.

The correlation function for doubly strange $J^P = 1^+$ $[ss]$ diquarks is defined analogously to (1) but with current

$$J_\alpha^{(\Gamma)}(x) \rightarrow J_\alpha^\mu(x) = \epsilon_{\alpha\beta\gamma} s_\beta(x) C\gamma^\mu s_\gamma(x). \qquad (5)$$

The axial-vector doubly strange diquark states are extracted as in (4). When discussing doubly strange diquarks, the left-hand side of (4) is denoted $\Pi^{[ss]}(Q^2)$.

The Schwinger string, schematically shown in Fig. 1, is given by

$$S_{\alpha\omega}(x,0) = \hat{P} \exp\left[ig_s \frac{\lambda^a}{2} \int_0^x dz^\mu A_\mu^a(z)\right]_{\alpha\omega}, \qquad (6)$$

where $\hat{P}$, the path-ordering operator, is used to extract gauge-invariant information from the correlation functions of the (gauge-dependent) diquark currents [49,50]. In principle, the Schwinger string could present calculational challenges for the correlation function, but there exist some important simplifications. In the Landau gauge, the straight-line string trajectory representing the ground-state configuration has zero perturbative contribution to the correlation function at NLO [49,50]. This was explicitly verified in Ref. [52] where the heavy-light diquark correlation function in Eq. (1) was calculated to NLO in an arbitrary covariant gauge and it was shown that the result is independent of the gauge parameter. Note that this same approach was used for doubly heavy $[QQ]$ diquarks in Ref. [55]. In this work, for completeness it has been verified that the same cancellation of the gauge parameter occurs for the heavy-strange $[Qs]$ and doubly strange $[ss]$ diquarks. Therefore perturbative contributions from the Schwinger string can be replaced by $S_{\alpha\omega}(x,0) \rightarrow \delta_{\alpha\omega}$ while working in Landau gauge up to NLO. Similarly, nonperturbative QCD condensate contributions from the Schwinger string are zero at LO in fixed-point gauge methods [49,50]. Combined with the equivalence between fixed-point gauge and other methods for calculating OPE coefficients for gauge-invariant correlators [62], nonperturbative

contributions from the Schwinger string can also be replaced by $S_{\alpha\omega}(x,0) \rightarrow \delta_{\alpha\omega}$ at LO.

The contributions to the heavy-light $[Qq]$ diquark correlation function are now calculated up to NLO in perturbation theory and up to LO in the strange quark mass m_s as shown in the Feynman diagrams of Fig. 2. The necessary heavy-light diquark composite operator renormalization properties are known to two-loop order [63] and were successfully implemented in the NLO light-quark chiral limit correlation function calculation of Ref. [52]. Here, the presence of an additional mass scale for strange quarks presents additional technical challenges in the renormalization of nonlocal (i.e., nonpolynomial in Q^2) divergences resulting from the diagrams of Fig. 2. These technical challenges are addressed via diagrammatic renormalization methods (see, e.g., Refs. [64–67]) for QCD correlation functions as discussed in Ref. [68].
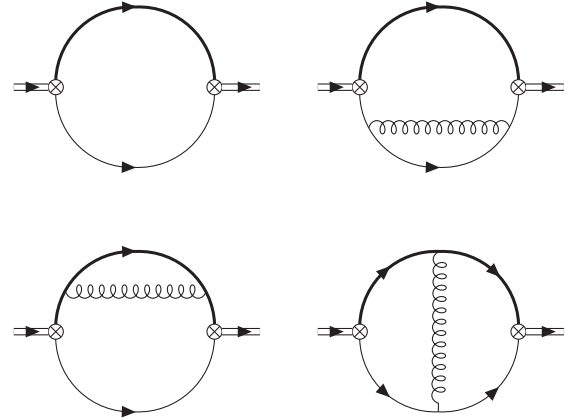
FIG. 2. LO and NLO Feynman diagrams for perturbative contributions to the correlation function for the heavy-light diquarks. Bold lines represent the heavy quark, thin lines represent the strange (for the $[Qs]$ diquark) or nonstrange (for the $[Qq]$ diquark) quarks, curly lines represent the gluon, and $\otimes$ indicates an insertion of the diquark current.

FIG. 3. Subdiagrams extracted from Fig. 2. Diagrams (a) and (b) originate from the self-energy topologies (top-right and bottom-left diagrams) in Fig. 2, while diagrams (c) and (d) originate from the gluon exchange topology (bottom-right) in Fig. 2.
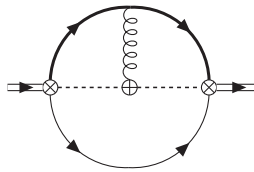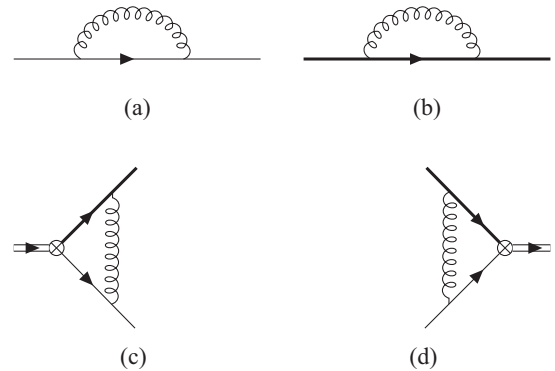

FIG. 1. Feynman diagram representing the LO contribution to the Schwinger string (6) for a straight-line spacetime trajectory (dashed-line) between spacetime points x and 0 represented by the diquark current insertions $\otimes$, with $\oplus$ representing z. A similar diagram also occurs with the gluon connecting to the light quark line.
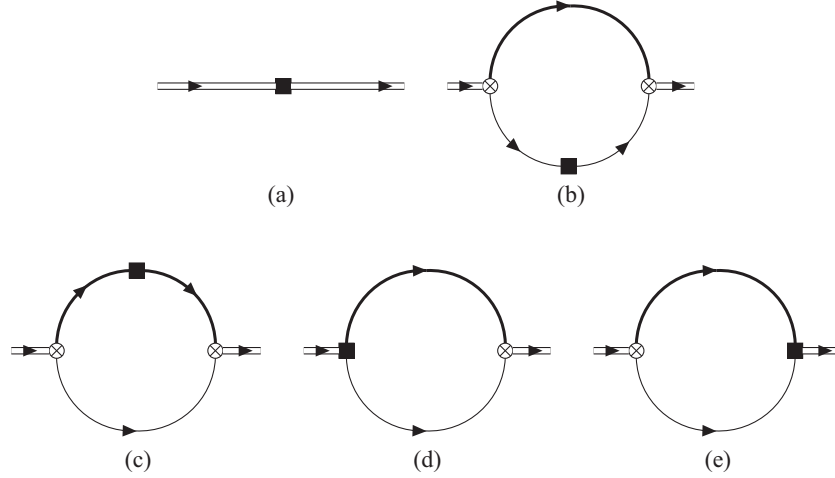
FIG. 4.   Counterterm diagrams generated by the subdiagrams of Fig. 3 and associated with the corresponding diagrams of Fig. 2, where the "black square" represents the subdivergence insertion. Diagram (b) is the counterterm for the top-right (self-energy) diagram of Fig. 2, diagram (c) is for the bottom-left (self-energy) diagram of Fig. 2, and diagrams (d),(e) are for the bottom-right (gluon exchange) diagram of Fig. 2. For completeness, diagram (a) shows the counterterm for the LO diagram (top-left diagram) of Fig. 2 and results in a local divergence corresponding to a dispersion relation subtraction that does not contribute to QCD sum rules.

For each of the bare NLO diagrams of Fig. 2, the first step in diagrammatic renormalization is calculating the divergent part of the subdiagrams shown in Fig. 3. These subdivergences are then used to construct the counterterm diagrams of Fig. 4. The counterterm diagrams are calculated and then subtracted from the original diagram, resulting in the renormalized diagram where the strong coupling α_s and quark masses m are interpreted as $\alpha_s(\mu)$ and $m(\mu)$ at renormalization scale μ in the desired renormalization scheme. This diagrammatic renormalization process cancels all nonlocal divergences from the original diagram; the remaining local divergences are polynomials in Q^2 corresponding to dispersion relation subtractions which are removed while constructing the QCD sum rules (e.g., via the Borel transform). Note that the subdiagram and associated counterterm diagram of Fig. 5 result in local divergences and can therefore be ignored as a

dispersion-relation subtraction that does not contribute to the sum rules. Detailed examples, technical subtleties, and computational advantages of the diagrammatic renormalization procedure for QCD correlation functions are outlined in Ref. [68] along with the conceptual connection to conventional operator mixing renormalization methods.

Calculation of the correlation functions is performed using dimensional regularization with $D = 4 + 2\epsilon$, and final results are presented in the $\overline{\text{MS}}$ scheme.[2] Feynman diagrams are calculated using FeynCalc [69–71], TARCER [72] implementation of recursion relations for two-loop integrals [73,74], Package-X [75,76], results for master integrals [77–79], and HypExp [80,81], with HPL [82] for the expansion of hypergeometric functions.

The renormalized final result for the perturbative contributions to NLO in the loop expansion and to first-order in the strange quark mass is given by

$$
\begin{aligned}
\Pi_{\text{pert}}^{(\Gamma)}(Q^2) = \frac{m^2}{\pi^2}\frac{w+1}{w^2}\Bigg[& \left(c_0 + \frac{m_s}{m}d_0\right)\log(1+w) + \frac{\alpha_s}{\pi}\Bigg[\left(c_1 + \frac{m_s}{m}d_1\right)\log(1+w) + \left(c_2 + \frac{m_s}{m}d_2\right)\log^2(1+w) \\
& + \left(c_3 + \frac{m_s}{m}d_3\right)\log^3(1+w) + \left(c_4 + \frac{m_s}{m}d_4\right)\log(1+w)\text{Li}_2\left(\frac{w}{1+w}\right) + \left(c_5 + \frac{m_s}{m}d_5\right)\text{Li}_2\left(\frac{w}{1+w}\right) \\
& + \left(c_6 + \frac{m_s}{m}d_6\right)\text{Li}_3(-w) + \left(c_7 + \frac{m_s}{m}d_7\right)\text{Li}_3\left(\frac{w}{1+w}\right)\Bigg]\Bigg],
\end{aligned}
\tag{7}
$$

$$
w = \frac{Q^2}{m^2},
\tag{8}
$$

---

[2] It is easiest to carry out diagrammatic renormalization in MS scheme and then convert to $\overline{\text{MS}}$ by redefinition of the renormalization scale $\mu^2 \to \frac{e^{\gamma_E}}{4\pi}\mu^2$.
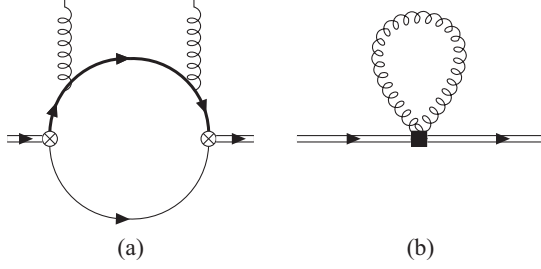
FIG. 5. Additional subdiagram (a) and counterterm diagram (b) originating from the quark loops in the self-energy topologies (top right and bottom left) of Fig. 2. The counterterm diagram results in a local divergence corresponding to a dispersion relation subtraction that does not contribute to QCD sum rules.

where m is the heavy quark mass, and $\Gamma \in \{P, S, A, V\}$ indicates the quantum numbers of the current. The quantities m, m_s, and α_s are implicitly referenced to the renormalization scale μ in the $\overline{\text{MS}}$ scheme. The coefficients c_i and d_i are functions of $w = Q^2/m^2$ (with $Q^2 = -q^2$) given in Tables I and II. The agreement between c_0 to c_7 in

Table I with Table 2 of Ref. [52] validates the diagrammatic renormalization methodology. As discussed above, in obtaining (7), it has been verified that the gauge parameter cancels from the Schwinger string up to first order in m_s, extending the chiral-limit analysis of [52] and justifying the use of Landau gauge where the Schwinger string is simplified to the color-space identity operator $\delta_{\alpha\omega}$ [49,50]. The new results in (7) are the strange-quark mass corrections d_0 to d_7 given in Table II. Higher-order terms proportional to $(m_s/m)^2$ are numerically suppressed by the small value of the strange-heavy quark mass ratio m_s/m. Additional details showing the explicit cancellation of divergences in the diagrammatic renormalization for diquark correlation functions are given in Ref. [68].

The QCD spectral function (imaginary part) associated with $\Pi^{(\Gamma)}(Q^2)$ is required to formulate the Laplace sum rules (see, e.g., detailed discussion in Ref. [83]). Analytic continuation of (7) leads to the following imaginary part of the perturbative contributions (see, e.g., Refs. [84,85] for conventions and details)

$$
\begin{aligned}
\text{Im}\Pi_{\text{pert}}^{(\Gamma)}(x) = \frac{m^2}{4\pi x}&\left[\left(f_0 + \frac{m_s}{m}g_0\right) + \frac{\alpha_s}{\pi}\left[\left(f_1 + \frac{m_s}{m}g_1\right) + \left(f_2 + \frac{m_s}{m}g_2\right)\log(x) + \left(f_3 + \frac{m_s}{m}g_3\right)\log(1-x)\right.\right.\\
&\left.\left.+ \left(f_4 + \frac{m_s}{m}g_4\right)\log(x)\log(1-x) + \left(f_5 + \frac{m_s}{m}g_5\right)\text{Li}_2(x) + \left(f_6 + \frac{m_s}{m}g_6\right)\log\left(\frac{m^2}{\mu^2}\right)\right]\right], \qquad 0 < x < 1,
\end{aligned}
\tag{9}
$$

$$
x = \frac{m^2}{t} = \frac{m^2}{q^2}.
\tag{10}
$$

The coefficients f_i and g_i are functions of x given in Tables III and IV. The coefficients f_0 to f_7 in Table III agree with Table 3 of Ref. [52], providing a consistency check on the extraction of the imaginary parts. The new results in (9)

are the strange-quark mass corrections g_0 to g_7 in Table IV. Similarly, the new results in (7) are the strange-quark mass corrections d_0 to d_7 in Table II. Thus the NLO perturbative contributions to the benchmark heavy-nonstrange $[Qn]$ diquark sum rules can be formulated by ignoring the Eq. (9) g_i coefficients, or the Eq. (7) d_i coefficients, (i.e., in the chiral limit) and the new analysis of heavy-strange

TABLE I. Coefficient functions c_i for the renormalized perturbative result (7). Note that $L_m = \log(\frac{m^2}{\mu^2})$, where μ is the renormalization scale. The coefficients agree with Table 2 of Ref. [52], providing a valuable confirmation of the diagrammatic renormalization methods. The definition of w is given in (8).

J^P	$0^{\pm}$ (S, P)	$1^{\pm}$ (A, V)
c_0	$\frac{3}{4}w(1+w)$	$\frac{1}{4}(1+w)(2w-1)$
c_1	$\frac{w}{24}[165 + 51w + 2\pi^2(1+w) - 18(5+w)L_m]$	$\frac{1}{36}[9w^2 + 90w - 93 - \pi^2(2w^2 + w - 1) - 54(w-1)L_m]$
c_2	$-\frac{2 + 12w + 16w^2 + 3w^3}{8(1+w)}$	$\frac{4 + 2w - 7w^2}{12(1+w)}$
c_3	$\frac{1}{4}w(1+w)$	$\frac{1}{12}(1+w)(2w-1)$
c_4	$w(1+w)$	$\frac{1}{3}(1+w)(2w-1)$
c_5	$\frac{w^2(2+5w)}{4(1+w)}$	$\frac{5w^3 - w^2 - w}{6(1+w)}$
c_6	$\frac{3}{2}w(1+w)$	$\frac{1}{2}(1+w)(2w-1)$
c_7	$\frac{3}{2}w(1+w)$	$\frac{1}{2}(1+w)(2w-1)$

TABLE II.   Coefficient functions d_i for the renormalized perturbative result (7). Note that $L_m = \log(\frac{m^2}{\mu^2})$, where μ is the renormalization scale. The definition of w is given in (8).

J^P	$0^{\mp}$ (P,S)	$1^{\mp}$ (V,A)
d_0	$\pm\frac{3}{2}w$	$\pm\frac{3}{2}w$
d_1	$\pm\frac{w[-9(3w+5)L_m+63w+\pi^2(w+1)+87]}{6(w+1)}$	$\pm\frac{-36w(w+2)L_m+(93+2\pi^2)w^2+2w(72+\pi^2)+3}{12(w+1)}$
d_2	$\mp\frac{9w^2+16w+2}{4(w+1)}$	$\mp\frac{6w^2+10w-1}{4(w+1)}$
d_3	$\pm\frac{w}{2}$	$\pm\frac{w}{2}$
d_4	$\pm 2w$	$\pm 2w$
d_5	$\pm\frac{5w^2}{2(w+1)}$	$\pm\frac{5w^2}{2(w+1)}$
d_6	$\pm 3w$	$\pm 3w$
d_7	$\pm 3w$	$\pm 3w$

$[Qs]$ sum rules (to first order in the strange-heavy quark mass ratio m_s/m) is obtained by including both the f_i and g_i coefficients from (9).

Regarding doubly strange diquarks, the perturbative diagrams that contribute to $\Pi^{[ss]}(Q^2)$ up to NLO are those shown in Fig. 2 but with all quark lines representing strange quarks. In this case, the upper-right and lower-left diagrams of Fig. 2 are degenerate. Unlike the $[Qs]$ case

TABLE III.   Coefficient functions f_i for the imaginary part of the renormalized perturbative result (9), where x is defined in (10). The coefficients agree with Table 3 of Ref. [52], providing a valuable confirmation of the diagrammatic renormalization methods.

J^P	$0^{\pm}$ (S,P)	$1^{\pm}$ (A,V)
f_0	$3(1-x)^2$	$2-3x+x^3$
f_1	$\frac{1}{2}(17-72x+55x^2)$	$\frac{1}{3}(3-33x-x^2+31x^3)$
f_2	$3-16x+12x^2-2x^3$	$\frac{2}{3}x(-7-2x+4x^2)$
f_3	$2(x-4)(1-x)^2$	$-\frac{2}{3}(1-x)^2(5+4x)$
f_4	$2(1-x)^2$	$\frac{2}{3}(2-3x+x^3)$
f_5	$4(1-x)^2$	$\frac{4}{3}(2-3x+x^3)$
f_6	$-3(1-6x+5x^2)$	$6x(1-x^2)$

TABLE IV.   Coefficient functions g_i for the imaginary part of the renormalized perturbative result (9), where x is defined in (10).

J^P	$0^{\mp}$ (P,S)	$1^{\mp}$ (V,A)
g_0	$\pm 6x(x-1)$	$\pm 6x(x-1)$
g_1	$\pm(58x^2-42x)$	$\pm(-x^3+48x^2-31x)$
g_2	$\pm(-4x^3+32x^2-18)x$	$\pm 2x(x^2+10x-6)$
g_3	$\pm 4x(x-1)(x-7)$	$\pm 2x(1-x)(x+11)$
g_4	$\pm 4x(x-1)$	$\pm 4x(x-1)$
g_5	$\pm 8x(x-1)$	$\pm 8x(x-1)$
g_6	$\pm 6x(3-5x)$	$\pm 12x(1-2x)$

where the heavy quark mass scale m can combine with m_s to obtain an $\mathcal{O}(m_s)$ correction, for $[ss]$ diquarks it is necessary to work to $\mathcal{O}(m_s^2)$ to find the strange quark mass corrections. As discussed above, following the Ref. [55] analysis of $[QQ]$ diquarks, the gauge parameter also cancels for $[ss]$ diquarks, the Schwinger string is trivial in Landau gauge [49,50], and up to $\mathcal{O}(m_s^2)$ the NLO perturbative result is

$$\Pi^{[ss]}_{\text{pert}}(Q^2) = \frac{Q^2}{\pi^2}\left[1+\frac{\alpha_s}{2\pi}\left(1-\frac{45m_s^2}{Q^2}\right)\right]\log\left(\frac{Q^2}{\mu^2}\right). \quad (11)$$

Note that the $\mathcal{O}(m_s^2)$ correction to LO perturbation theory vanishes. Renormalization is trivial as (11) is finite, consistent with the absence of LO m_s corrections and the result of Ref. [63] in which it was shown that the axial vector diquark current multiplicative renormalization constant is $1+\mathcal{O}(\alpha_s^2)$. It is then straightforward to show that

$$\text{Im}\Pi^{[ss]}_{\text{pert}}(t) = \frac{t}{\pi}\left[1+\frac{\alpha_s}{2\pi}\left(1-\frac{45m_s^2}{t}\right)\right]. \quad (12)$$

The QCD condensate contributions to the heavy-light diquark correlation functions are now considered. As discussed above, fixed-point gauge techniques are used because of the simplification that the Schwinger string reduces to the identity operator for the $x^\mu A^a_\mu = 0$ fixed-point gauge condition [49,50]. Furthermore, the gauge invariance of the correlation function (1) implies that fixed-point gauge methods will be equivalent to those obtained in other methods [62], justifying the use of the Schwinger-string simplification.

QCD condensate contributions to the heavy-light diquark correlation functions do not require light-quark mass corrections beyond leading order.[3] Such m_s/m effects would be numerically smaller than uncertainties in the

---

[3]Mixing of scalar glueballs and $\bar{q}q$ mesons are one example where light-quark mass corrections are necessary [86,87].

FIG. 6. Feynman diagram for dimension-three $\langle \bar{q}q \rangle$ quark condensate contributions to the heavy-light diquark correlation function (1).

QCD condensate parameters and would introduce significant operator mixing complications into the calculation of OPE coefficients [88,89]. Thus, in principle, the QCD condensate results [52] can be interpreted as applying to any light-quark mass m_q and with appropriate input of the QCD condensates (e.g., nonstrange systems where $\langle \bar{q}q \rangle = \langle \bar{n}n \rangle$ and strange systems where $\langle \bar{q}q \rangle = \langle \bar{s}s \rangle$). The QCD condensate results of [52] are extended to include some minor effects of additional Feynman diagrams as outlined below.

The Feynman diagram for the dimension-three $\langle \bar{q}q \rangle = \langle \bar{q}_i^\beta q_i^\beta \rangle$ quark condensate contributions to the diquark correlation function is shown in Fig. 6, and the result is [52]

$$
\Pi_{\langle \bar{q}q \rangle}^{(S,A)}(Q^2) = -\frac{2m \langle \bar{q}q \rangle}{Q^2 + m^2},
$$
$$
\Pi_{\langle \bar{q}q \rangle}^{(P,V)}(Q^2) = -\Pi_{\langle \bar{q}q \rangle}^{(S,A)}(Q^2). \tag{13}
$$

As discussed above, Eq. (13) can be applied to both nonstrange and strange heavy-light diquarks through input of the appropriate value of $\langle \bar{q}q \rangle$.

For $[ss]$ diquarks, the diagram that gives the dimension-three quark condensate contribution to $\Pi^{[ss]}(Q^2)$ is that of Fig. 6 but, again, with all quark lines representing strange quarks. To $\mathcal{O}(m_s)$, the result is

$$
\Pi_{\langle \bar{s}s \rangle}^{[ss]}(Q^2) = -\frac{8m_s \langle \bar{s}s \rangle}{Q^2}. \tag{14}
$$

The Feynman diagrams for the dimension-four $\langle \alpha_s G^2 \rangle = \langle \alpha_s G_{\mu\nu}^a G_{\mu\nu}^a \rangle$ gluon condensate contributions to the diquark correlation function are shown in Fig. 7, and the result is [52]

$$
\Pi_{\langle \alpha_s G^2 \rangle}^{(S,P)}(Q^2) = \frac{\langle \alpha_s G^2 \rangle}{24\pi} \frac{1}{Q^2 + m^2},
$$
$$
\Pi_{\langle \alpha_s G^2 \rangle}^{(A,V)}(Q^2) = \frac{\langle \alpha_s G^2 \rangle}{24\pi} \left[\frac{1}{Q^2} - \frac{3}{Q^2 + m^2} - \frac{m^2}{Q^4} \log\left(1 + \frac{Q^2}{m^2}\right) \right]. \tag{15}
$$

Note that the V, A channels have an imaginary part that is required to construct the QCD Laplace sum rules:

$$
\text{Im}\Pi_{\langle \alpha_s G^2 \rangle}^{(A,V)}(t) = \frac{\langle \alpha_s G^2 \rangle}{24m^2} x^2, \qquad 0 < x < 1, \tag{16}
$$

where x is defined in (10).

For $\Pi^{[ss]}(Q^2)$, the diagrams corresponding to the dimension-four gluon condensate contribution are those of Fig. 7. Again, all quark lines should be interpreted as strange quarks. In this case, the first two diagrams of Fig. 7 are degenerate. Summing all diagrams gives

$$
\Pi_{\langle \alpha_s G^2 \rangle}^{[ss]}(Q^2) = -\frac{\langle \alpha_s G^2 \rangle}{6\pi Q^2}. \tag{17}
$$

The Feynman diagrams for the dimension-five $\langle g\bar{q}\sigma Gq \rangle = \langle g\bar{q} \frac{\lambda^a}{2} \sigma^{\mu\nu} G_{\mu\nu}^a q \rangle$ mixed condensate contributions to the diquark correlation function are shown in Fig. 8, extending the calculations of Ref. [52] with the inclusion of diagram (b), resulting in

$$
\Pi_{\langle g\bar{q}\sigma Gq \rangle}^{(S)}(Q^2) = \frac{m(m^2 - Q^2)}{2(Q^2 + m^2)^3} \langle g\bar{q}\sigma Gq \rangle,
$$
$$
\Pi_{\langle g\bar{q}\sigma Gq \rangle}^{(P)}(Q^2) = -\Pi_{\langle g\bar{q}\sigma Gq \rangle}^{(S)}(Q^2),
$$
$$
\Pi_{\langle g\bar{q}\sigma Gq \rangle}^{(A)}(Q^2) = \frac{m^3}{(Q^2 + m^2)^3} \langle g\bar{q}\sigma Gq \rangle,
$$
$$
\Pi_{\langle g\bar{q}\sigma Gq \rangle}^{(V)}(Q^2) = -\Pi_{\langle g\bar{q}\sigma Gq \rangle}^{(A)}(Q^2). \tag{18}
$$

As for the $\langle \bar{q}q \rangle$ contributions, Eq. (18) can be applied to both nonstrange and strange heavy-light diquarks through input of the appropriate value of $\langle g\bar{q}\sigma Gq \rangle$.

The dimension-five mixed condensate contributions to $\Pi^{[ss]}(Q^2)$ are given by the diagrams of Fig. 8 but, again,
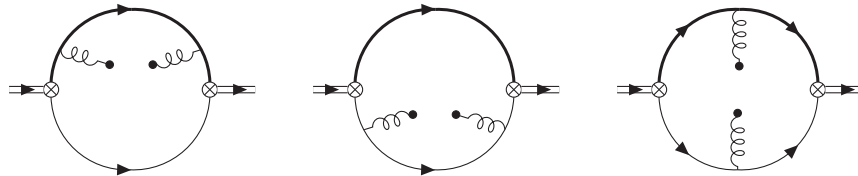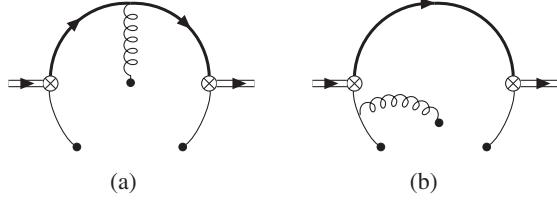

FIG. 7. Feynman diagrams for the dimension-four $\langle \alpha_s G^2 \rangle$ gluon condensate contributions to the heavy-light diquark correlation function (1).

(a)   (b)

FIG. 8. Feynman diagrams for the dimension-five $\langle g\bar{q}\sigma Gq\rangle$ mixed condensate contributions to the heavy-light diquark correlation function (1).
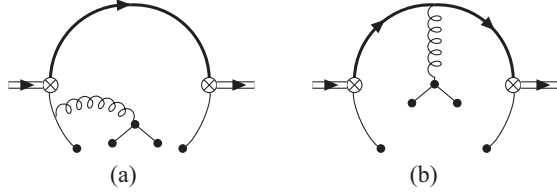

(a)   (b)

FIG. 9. Feynman diagrams for the dimension-six $\langle \bar{q}q\bar{q}q\rangle$ quark condensate contributions to the heavy-light diquark correlation function (1).

with all quark lines representing strange quarks. Summing the two diagrams gives

$$\Pi^{[ss]}_{\langle g\bar{s}\sigma Gs\rangle}(Q^2) = \frac{m_s}{3Q^4}\langle g\bar{s}\sigma Gs\rangle. \tag{19}$$

The Feynman diagrams for the dimension-six $\langle \bar{q}q\bar{q}q\rangle$ quark condensate contributions to the diquark correlation function are shown in Fig. 9, extending the calculations of Ref. [52] with inclusion of diagram (b), resulting in

$$\Pi^{(S,P)}_{\langle \bar{q}q\bar{q}q\rangle}(Q^2) = \frac{8\pi}{27}\frac{m^4 - 3m^2Q^2 - 2Q^4}{(Q^2+m^2)^4}\alpha_s\langle \bar{q}q\rangle^2,$$

$$\Pi^{(A,V)}_{\langle \bar{q}q\bar{q}q\rangle}(Q^2) = -\frac{4\pi}{27}\frac{5m^4 + 12m^2Q^2 + 3Q^4}{(Q^2+m^2)^4}\alpha_s\langle \bar{q}q\rangle^2. \tag{20}$$

where the vacuum saturation approximation [43,44] has been used for the various dimension-six quark condensates. With appropriate input of the condensate parameter $\alpha_s\langle \bar{q}q\rangle^2$, Eq. (20) can be applied to both nonstrange and strange heavy-light diquarks.

The diagrams that contribute to the dimension-six quark condensate part of $\Pi^{[ss]}(Q^2)$ are those of Fig. 9 with all quark lines representing strange quarks and the diagram shown in Fig. 10. The extra diagram of Fig. 10 does not contribute to the heavy-light diquark correlator as it would require a heavy quark line to condense. Summing all diagrams gives, to $\mathcal{O}(m_s)$,

$$\Pi^{[ss]}_{\langle \bar{s}s\bar{s}s\rangle}(Q^2) = \frac{32\pi}{3Q^4}\alpha_s\langle \bar{s}s\rangle^2. \tag{21}$$
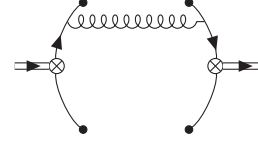

FIG. 10. Feynman diagram for the dimension-six $\langle \bar{s}s\bar{s}s\rangle$ condensate that contributes to the doubly strange diquark correlation function but not the heavy-light diquark correlation function.

As in (20), the vacuum saturation hypothesis has been used in (21).

III. QCD LAPLACE SUM-RULE ANALYSIS

Formulation of the QCD Laplace sum-rules begins with the dispersion relation satisfied by (1)

$$\Pi^{(\Gamma)}(Q^2) = \Pi(0) + Q^2\Pi'(0) + Q^4\int_{t_0}^{\infty}\frac{\rho_\Gamma(t)}{t^2(t+Q^2)}dt, \tag{22}$$

where $\rho_\Gamma(t)$ is the spectral function with threshold t_0 related to states $|h\rangle$ with quantum numbers such that the current $J^{(\Gamma)}$ serves as an interpolating field to the vacuum $\langle h|J^{(\Gamma)}|\Omega\rangle \neq 0$. In (22), Γ can represent a heavy-light or a doubly strange diquark. The (divergent) subtraction constants $\Pi(0)$ and $\Pi'(0)$ can be eliminated and the ground state can be enhanced in (22) through the Borel transform operator $\hat{B}$ [43,44]

$$\hat{B} \equiv \lim_{\substack{N,Q^2\to\infty \\ N/Q^2\equiv\tau}}\frac{(-Q^2)^N}{\Gamma(N)}\left(\frac{d}{dQ^2}\right)^N, \tag{23}$$

which has the useful properties

$$\hat{B}[a_0 + a_1Q^2 + \ldots a_nQ^{2n}] = 0, \quad n = 0,1,2,\ldots \quad (n\text{ finite}), \tag{24}$$

$$\hat{B}\left[\frac{Q^{2n}}{t+Q^2}\right] = \tau(-1)^n t^n e^{-t\tau}, \quad n = 0,1,2,\ldots. \tag{25}$$

The Borel transform $\hat{B}$ is related to the inverse Laplace transform [90] via

$$f(Q^2) = \int_0^{\infty}F(\tau)e^{-Q^2\tau}d\tau \equiv \mathcal{L}[F(\tau)]$$

$$\Rightarrow \frac{1}{\tau}\hat{B}[f(Q^2)] = F(\tau) = \mathcal{L}^{-1}[f(Q^2)], \tag{26}$$

$$\mathcal{L}^{-1}[f(Q^2)] = \frac{1}{2\pi i}\int_{b-i\infty}^{b+i\infty}f(Q^2)e^{Q^2\tau}dQ^2, \tag{27}$$

where the real parameter b in the definition (27) of the inverse Laplace transform must be chosen so that $f(Q^2)$ is

analytic to the right of the contour of integration in the complex Q^2 plane. In cases where the correlation function has an imaginary part branch cut discontinuity (e.g., perturbative and gluon condensate contributions discussed above) the Borel transform results in an integration of the imaginary part representing the QCD spectral function (see e.g., Ref. [83]) that ultimately gets combined with the continuum contributions as discussed below.

Laplace sum rules are obtained by applying $\hat{B}$ to (22) weighted by integer powers of Q^2, which will involve the QCD prediction

$$\mathcal{L}_k^{(\Gamma)}(\tau) \equiv \frac{1}{\tau} \hat{B}[(-1)^k Q^{2k} \Pi^{(\Gamma)}(Q^2)]$$
$$= \mathcal{L}^{-1}[(-1)^k Q^{2k} \Pi^{(\Gamma)}(Q^2)]. \qquad (28)$$

For $k \geq 0$, this results in the following Laplace sum rules relating the QCD prediction $\mathcal{L}_k^{(\Gamma)}(\tau)$ to the spectral function $\rho_\Gamma(t)$

$$\mathcal{L}_k^{(\Gamma)}(\tau) = \int_{t_0}^{\infty} t^k e^{-t\tau} \rho_\Gamma(t) \mathrm{d}t, \qquad k \geq 0. \qquad (29)$$

The high-energy region in (29) is suppressed by the exponential factor, which enhances the low-energy states of the spectral function. The spectral function is now separated into a resonance contribution and a QCD continuum (see, e.g., Refs. [43–48])

$$\rho_\Gamma(t) = \rho_\Gamma^{\mathrm{res}}(t) + \theta(t - s_0) \frac{1}{\pi} \mathrm{Im}\Pi^{(\Gamma)}(t), \qquad (30)$$

$$c_k^{(\Gamma)}(\tau, s_0) = \int_{s_0}^{\infty} t^k e^{-t\tau} \frac{1}{\pi} \mathrm{Im}\Pi^{(\Gamma)}(t) dt, \qquad (31)$$

leading to a family of Laplace sum rules relating the QCD prediction $\mathcal{R}_k(\tau, s_0)$ to resonance contributions $\rho_\Gamma^{\mathrm{res}}(t)$

$$\mathcal{R}_k^{(\Gamma)}(\tau, s_0) = \mathcal{L}_k^{(\Gamma)}(\tau) - c_k(\tau, s_0), \qquad (32)$$

$$\mathcal{R}_k^{(\Gamma)}(\tau, s_0) = \int_{t_0}^{s_0} t^k e^{-t\tau} \rho_\Gamma^{\mathrm{res}}(t) dt. \qquad (33)$$

The exponential factor in Eqs. (31) and (33) has a combined effect of enhancing the ground state resonance and suppressing the QCD continuum.

The imaginary parts needed to calculate the continuum contributions are given in Eqs. (9), (12), and (16) (see also Tables III and IV). The Borel transform of the QCD condensate contributions to (28) are denoted by

$$B_{\mathrm{cond}}^{(\Gamma)}(k, \tau) \equiv \frac{\hat{B}}{\tau} \left[(-Q^2)^k \Pi_{\mathrm{cond}}^{(\Gamma)}(Q^2) \right]. \qquad (34)$$

Beginning with heavy-light diquarks and using (25) for the results in Eqs. (13), (15), (18), (20) gives

$$B_{\langle \bar{q}q \rangle}^{(S,A)}(k, \tau) = -2m \langle \bar{q}q \rangle m^{2k} e^{-m^2 \tau},$$
$$B_{\langle \bar{q}q \rangle}^{(P,V)}(k, \tau) = -B_{\langle \bar{q}q \rangle}^{(S,A)}(k, \tau) \qquad (35)$$

for the $\langle \bar{q}q \rangle$ terms,

$$B_{\langle \alpha_s G^2 \rangle}^{(S,P)}(k, \tau) = \frac{\langle \alpha_s G^2 \rangle}{24\pi} m^{2k} e^{-m^2 \tau},$$
$$B_{\langle \alpha_s G^2 \rangle}^{(A,V)}(k, \tau) = -\frac{\langle \alpha_s G^2 \rangle}{8\pi} m^{2k} e^{-m^2 \tau}, \qquad (36)$$

for the $\langle \alpha_s G^2 \rangle$ terms [note the logarithmic term in (15) that contributes to the inverse Laplace Borel transform will be combined with the continuum contribution],

$$B_{\langle g\bar{q}\sigma Gq \rangle}^{(S)}(k, \tau) = \frac{1}{2} m \langle g\bar{q}\sigma Gq \rangle (m^2)^{k-1}$$
$$\times e^{-m^2\tau}[k^2 - 2km^2\tau + m^2\tau(m^2\tau - 1)],$$

$$B_{\langle g\bar{q}\sigma Gq \rangle}^{(P)}(k, \tau) = -B_{\langle g\bar{q}\sigma Gq \rangle}^{(S)}(k, \tau),$$

$$B_{\langle g\bar{q}\sigma Gq \rangle}^{(A)}(k, \tau) = \frac{1}{2} m \langle g\bar{q}\sigma Gq \rangle (m^2)^{k-1}$$
$$\times e^{-m^2\tau} \left[\frac{k^2}{m^4} - \frac{k(2m^2\tau + 1)}{m^4} + \tau^2 \right],$$

$$B_{\langle g\bar{q}\sigma Gq \rangle}^{(V)}(k, \tau) = -B_{\langle g\bar{q}\sigma Gq \rangle}^{(A)}(k, \tau), \qquad (37)$$

for the $\langle g\bar{q}\sigma Gq \rangle$ terms, and

$$B_{\langle \bar{q}q\bar{q}q \rangle}^{(S,P)}(k, \tau) = \frac{4\pi}{81} \alpha_s \langle \bar{q}q \rangle^2 (m^2)^{k-1} e^{-m^2\tau} [-2k^3 + k^2(6m^2\tau + 9) + k(-6m^4\tau^2 - 12m^2\tau + 5) + m^2\tau(2m^4\tau^2 + 3m^2\tau - 12)],$$

$$B_{\langle \bar{q}q\bar{q}q \rangle}^{(A,V)}(k, \tau) = -\frac{4\pi}{81} \alpha_s \langle \bar{q}q \rangle^2 (m^2)^{k-1} e^{-m^2\tau} [2k^3 + k^2(3 - 6m^2\tau) + 2k(3m^4\tau^2 - 6m^2\tau - 7) + m^2\tau(-2m^4\tau^2 + 9m^2\tau + 9)],$$

$$\tag{38}$$

for the $\langle \bar{q}q\bar{q}q \rangle$ terms. Thus the final form of the Laplace sum rules $\mathcal{R}_k(\tau, s_0)$ is

$$\mathcal{R}_k^{(\Gamma)}(\tau, s_0) \equiv \sum_{\text{cond}} B_{\text{cond}}^{(\Gamma)}(k, \tau) - \frac{1}{\pi} \int_{s_0}^{\infty} t^k e^{-t\tau} \text{Im}\Pi^{(\Gamma)}(t) dt,$$

$$= B_{\langle \bar{q}q \rangle}^{(\Gamma)}(k, \tau) + B_{\langle \alpha_s G^2 \rangle}^{(\Gamma)}(k, \tau) + B_{\langle \bar{q}Gq \rangle}^{(\Gamma)}(k, \tau) + B_{\langle \bar{q}q\bar{q}q \rangle}^{(\Gamma)}(k, \tau)$$

$$+ \frac{m^2}{\pi} \int_{1}^{s_0/m^2} (m^2 z)^k \left[\text{Im}\Pi_{\text{pert}}^{(\Gamma)}\left(\frac{1}{z}\right) + \text{Im}\Pi_{\langle \alpha_s G^2 \rangle}^{(\Gamma)}\left(\frac{1}{z}\right) \right] dz. \tag{39}$$

Focusing second on $[ss]$ diquarks, Eqs. (14), (17), (19), (21), (25), and (34) together give

$$B_{\text{cond}}^{[ss]}(0, \tau) = -8m_s \langle \bar{s}s \rangle - \frac{\langle \alpha_s G^2 \rangle}{6\pi} + \tau \left(\frac{1}{3} m_s \langle g\bar{s}\sigma Gs \rangle + \frac{32\pi}{3} \alpha_s \langle \bar{s}s \rangle^2 \right), \tag{40}$$

$$B_{\text{cond}}^{[ss]}(1, \tau) = -\frac{1}{3} m_s \langle g\bar{s}\sigma Gs \rangle - \frac{32\pi}{3} \alpha_s \langle \bar{s}s \rangle^2. \tag{41}$$

Combining (12) and (32), the doubly strange Laplace sum rules are

$$\mathcal{R}_0^{[ss]}(\tau, s_0) = B_{\text{cond}}^{[ss]}(0, \tau) + \frac{1}{\pi^2 \tau^2} \left\{ 1 - e^{-s_0 \tau}(1 + s_0 \tau) + \frac{\alpha_s}{2\pi}[1 - e^{-s_0 \tau}(1 + s_0 \tau) - 45m_s^2 \tau(1 - e^{-s_0 \tau})] \right\}, \tag{42}$$

$$\mathcal{R}_1^{[ss]}(\tau, s_0) = B_{\text{cond}}^{[ss]}(1, \tau) + \frac{1}{\pi^2 \tau^3} \left\{ 2 - e^{-s_0 \tau}(2 + 2s_0 \tau + s_0^2 \tau^2) \right.$$

$$\left. + \frac{\alpha_s}{2\pi}[2 - e^{-s_0 \tau}(2 + 2s_0 \tau + s_0^2 \tau^2) - 45m_s^2 \tau(1 - e^{-s_0 \tau}[1 + s_0 \tau])] \right\}. \tag{43}$$

The QCD input parameters required for the sum rules will now be specified. The $\overline{\text{MS}}$ one-loop expression (see, e.g., Ref. [91]) for the strong coupling at scale μ, referenced to the Ref. [92] values of $\alpha_s(M_\tau)$ for charm heavy-light and doubly strange diquarks or $\alpha_s(M_Z)$ for bottom-light diquarks, is

$$\alpha_s(\mu) = \frac{\alpha_s(M)}{1 + A \frac{\alpha_s(M)}{\pi} \log\left(\frac{\mu^2}{M^2}\right)}, \tag{44}$$

where the parameters in (44) are specified in Table V. Note that the uncertainties in $\alpha_s(M_\tau)$ and $\alpha_s(M_Z)$ are negligibly small compared to other QCD inputs. Similarly, the (one-loop) $\overline{\text{MS}}$ heavy quark masses at scale μ is (see, e.g., Ref. [91])

$$\frac{m(\mu)}{\bar{m}} = \left(\frac{\alpha_s(\mu)}{\alpha_s(\bar{m})} \right)^{1/A}, \qquad \bar{m} = m(\mu = \bar{m}), \tag{45}$$

where $\bar{m}_c$ and $\bar{m}_b$ values from Ref. [93] are given in Table V. An analogous expression also applies to the strange quark mass anchored to $m_s(2 \text{ GeV}) = 93.4_{-3.4}^{+8.6}$ [93]

$$m_s(\mu) = m_s(2 \text{ GeV}) \left(\frac{\alpha_s(\mu)}{\alpha_s(2 \text{ GeV})} \right)^{1/A}, \quad A = \frac{25}{12}. \tag{46}$$

The result (46) is needed for the $[ss]$ Laplace sum rules (42) and (43). Because strange quark mass effects enter the $[Qs]$ perturbative results (7) as the renormalization group (RG) invariant strange/heavy mass ratio, the strange quark mass is parametrized for $[Qs]$ sum rules by

$$r_{Qs} = \frac{m(\mu)}{m_s(\mu)} = \frac{m(2 \text{ GeV})}{m_s(2 \text{ GeV})}, \tag{47}$$

with the Ref. [93] value for r_{Qs} given in Table V.

The Ref. [94] value for the $\langle \alpha_s G^2 \rangle$ gluon condensate will be used

$$\langle \alpha_s G^2 \rangle = (7.5 \pm 2.0) \times 10^{-2} \text{ GeV}^4. \tag{48}$$

The $\langle \bar{q}q \rangle$ quark condensate contributions enter with a prefactor of the heavy quark mass, so for the nonstrange

TABLE V. Parameters used for QCD sum-rule analysis, see text for details.

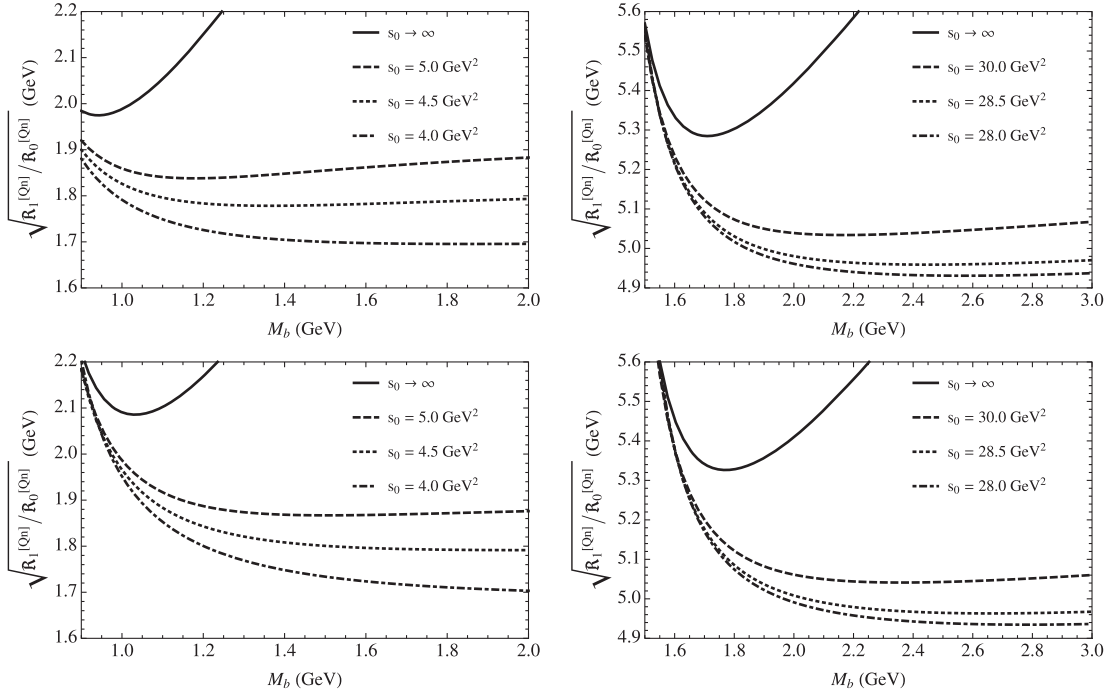| Parameter	Charm	Bottom
M (GeV)	$M_\tau = 1.77$	$M_Z = 91.188$
$\alpha_s(M)$	0.33 ± 0.01	0.1184 ± 0.0007
A	$25/12$	$23/12$
$\bar{m}$ (GeV)	1.27 ± 0.02	4.18 ± 0.03
r_{Qn}	321.40 ± 11.78	1474.18 ± 44.81
r_{Qs}	$11.76_{-0.10}^{+0.05}$	53.94 ± 0.12
κ	0.56, 0.66, 0.74, 0.80, 1.08	

FIG. 11. The sum-rule ratio $\sqrt{\mathcal{R}_1^{[Qn]}(M_b, s_0)/\mathcal{R}_0^{[Qn]}(M_b, s_0)}$ is shown as a function of the Borel scale M_b for 0^+ $[cn]$ (top left), 0^+ $[bn]$ (top right), 1^+ $[cn]$ (bottom left), and 1^+ $[bn]$ (bottom right) diquarks. Selected values of s_0 have been chosen near the optimized values s_0^{opt} of Table VI and for the $s_0 \to \infty$ robust upper bound on the mass prediction. The associated Borel windows for s_0^{opt} are given in Table VI.

condensate the RG-invariant PCAC Gell-Mann-Oakes-Renner relation [95]

$$m_n\langle \bar{n}n \rangle = -\frac{1}{2} f_\pi^2 m_\pi^2, \tag{49}$$

$$\langle \bar{n}n \rangle = \langle \bar{u}u \rangle = \langle \bar{d}d \rangle, \tag{50}$$

$$m_n(2 \text{ GeV}) = \frac{1}{2}[m_u(2 \text{ GeV}) + m_d(2 \text{ GeV})], \tag{51}$$

is combined with the nonstrange-heavy quark mass ratio to give the RG-invariant result

$$m\langle \bar{n}n \rangle = r_{Qn} m_n \langle \bar{n}n \rangle, \qquad r_{Qn} = \frac{m(2 \text{ GeV})}{m_n(2 \text{ GeV})}, \tag{52}$$

where the Ref. [93] value for r_{Qn} is given in Table V, the convention $f_\pi = 130/\sqrt{2}$ MeV [93] is used (along with $m_\pi = 0.139$ GeV), and Eq. (50) characterizes $SU(2)$ invariance of the vacuum. The $SU(3)$ flavor-breaking associated with the strange quark condensate is parametrized by the RG-invariant ratio

$$\kappa = \frac{\langle \bar{s}s \rangle}{\langle \bar{n}n \rangle}. \tag{53}$$

As shown below, κ is a crucial parameter in the $SU(3)$ flavor splitting of the QCD sum-rule mass predictions

for $[Qs]$ and $[Qn]$ diquarks.[4] Determinations of κ vary across a wide range, including QCD sum rules for mesonic systems [96–99], QCD sum rules for baryonic systems [61,100–102], lattice QCD [103], and combined lattice/sum-rule analyses [104] (see, e.g., Ref. [105] for a review). Table V specifies selected values from the conservative range $\kappa = 0.66 \pm 0.10$ of Ref. [46] obtained by combining mesonic and baryonic determinations, the $\kappa = 0.74$ central value of Ref. [102], the $\kappa = 0.8$ central value of Ref. [104], and the $\kappa = 1.08$ central value of Ref. [103]. Combining Eqs. (52) and (53) gives

$$m\langle \bar{s}s \rangle = m\kappa\langle \bar{n}n \rangle = \kappa r_{Qn} m_n \langle \bar{n}n \rangle. \tag{54}$$

Similarly, for the doubly strange $[ss]$ sum rules, the dimension-three quark condensate contribution is given by

$$m_s\langle \bar{s}s \rangle = m_s \kappa \langle \bar{n}n \rangle = \kappa r_{sn} m_n \langle \bar{n}n \rangle, \tag{55}$$

with [93]

$$r_{sn} = \frac{m_s(2 \text{ GeV})}{m_n(2 \text{ GeV})} = 27.33^{+0.67}_{-0.77}. \tag{56}$$

---

[4]Reference [47] discusses the importance of improving the determinations of κ.

TABLE VI. The optimized value for the continuum s_0^{opt} and the associated for J^P diquark mass predictions $M_{[Qn]}$ obtained by minimizing (71). The quantities M_b^{min} and M_b^{max} correspond to the Borel window obtained via Eqs. (69) and (68).

$[Qn]$	J^P	s_0^{opt} (GeV^2)	$M_{[Qn]}$ (GeV)	M_b^{min} (GeV)	M_b^{max} (GeV)
$[cn]$	0^+	4.50	1.78 ± 0.05	1.23	1.50
	1^+	5.00	1.87 ± 0.05	1.38	1.61
$[bn]$	0^+	28.5	4.97 ± 0.08	2.41	3.61
	1^+	28.5	4.97 ± 0.08	2.63	3.65

In $[Qq]$ and $[ss]$ sum rules, the mixed condensate $\langle g\bar{q}\sigma Gq \rangle$ also occurs with a quark-mass prefactor, so a similar approach as for the dimension-three quark condensates uses [106]

$$\langle g\bar{n}\sigma Gn \rangle = M_0^2 \langle \bar{n}n \rangle, \qquad M_0^2 = (0.8 \pm 0.1) \text{ GeV}^2 \quad (57)$$

to obtain

$$m\langle g\bar{n}\sigma Gn \rangle = r_{Qn} M_0^2 m_n \langle \bar{n}n \rangle, \quad (58)$$

$$m\langle g\bar{s}\sigma Gs \rangle = \kappa r_{Qn} M_0^2 m_n \langle \bar{n}n \rangle, \quad (59)$$

$$m_s\langle g\bar{s}\sigma Gs \rangle = \kappa r_{sn} M_0^2 m_n \langle \bar{n}n \rangle. \quad (60)$$

The dimension six $\langle \bar{n}n\bar{n}n \rangle$ condensate is given by [107]

$$\alpha_s \langle \bar{n}n\bar{n}n \rangle = (5.8 \pm 0.9) \times 10^{-4} \text{ GeV}^6, \quad (61)$$

which is extended to the strange case via (53) to give

$$\alpha_s \langle \bar{s}s\bar{s}s \rangle = \kappa^2 \alpha_s \langle \bar{n}n\bar{n}n \rangle$$
$$= \kappa^2 (5.8 \pm 0.9) \times 10^{-4} \text{ GeV}^6. \quad (62)$$

Having combined a factor of the heavy quark mass m with the chiral-violating condensates, a final subtlety in the $[Qq]$ sum-rule analysis involves the residual factors of the heavy quark mass appearing in the (LO) QCD condensate contributions. Following Refs. [52,108] the pole mass [108–112]

$$m = m(\mu)\left\{ 1 + \frac{\alpha_s(\mu)}{\pi}\left(\frac{4}{3} - \log\left[\frac{\bar{m}^2}{\mu^2} \right] \right) \right\} \quad (63)$$

and its relation to the $\overline{\text{MS}}$ mass $m(\mu)$ is used for these residual (LO) condensate mass factors. The final ingredient needed for the detailed QCD sum-rule analysis is RG-improvement, which is achieved by choosing the renormalization scale $\mu^2 = 1/\tau$ [113].

The methodology for using Eqs. (33), (39) to predict the heavy-light diquark mass spectrum begins with the narrow-resonance model

$$\rho_\Gamma^{\text{res}}(t) = f_\Gamma^2 \delta(t - M_\Gamma^2), \quad (64)$$

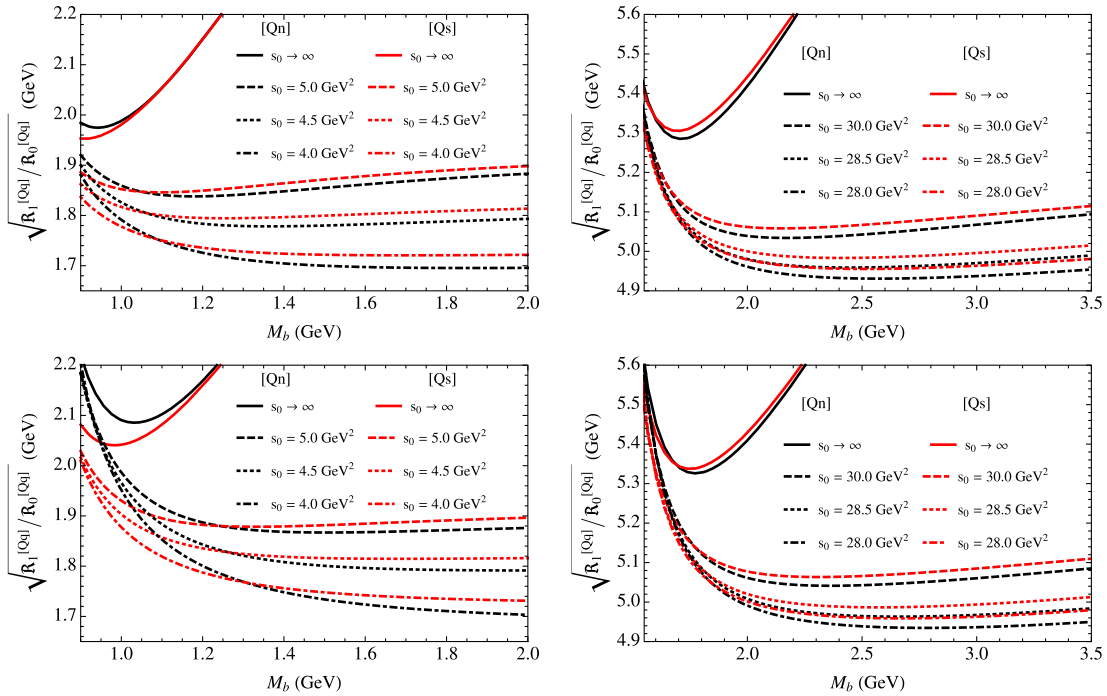FIG. 12. The quantity $\sqrt{\mathcal{R}_1^{[Qq]}(M_b, s_0)/\mathcal{R}_0^{[Qq]}(M_b, s_0)}$ for 0^+ $[cq]$ (top left), 0^+ $[bq]$ (top right), 1^+ $[cq]$ (bottom left), and 1^+ $[bq]$ (bottom right) diquarks for the s_0 values of Fig. 11 and with $\kappa = 0.74$. The black curves represent $[Qn]$ diquarks and the red curves represent $[Qs]$ diquarks.

where M_Γ is the heavy-light diquark mass with quantum numbers Γ and $f_\Gamma \sim \langle\Omega|J^{(\Gamma)}|h\rangle$ parametrizes the coupling of the diquark state $|h\rangle$ to the vacuum via the (interpolating field) current $J^{(\Gamma)}$. In this resonance model, (33) becomes

$$\mathcal{R}_k^{(\Gamma)}(\tau, s_0) = \frac{1}{\pi}\int_{t_0}^\infty t^k e^{-t\tau}\rho_\Gamma^{\mathrm{res}}(t)dt = f_\Gamma^2 M_\Gamma^{2k} e^{-M_\Gamma^2\tau}, \quad (65)$$

and the diquark mass M_Γ is related to the ratio of the two lowest-weight Laplace sum rules

$$\sqrt{\frac{\mathcal{R}_1^{(\Gamma)}(\tau, s_0)}{\mathcal{R}_0^{(\Gamma)}(\tau, s_0)}} = M_\Gamma, \quad (66)$$
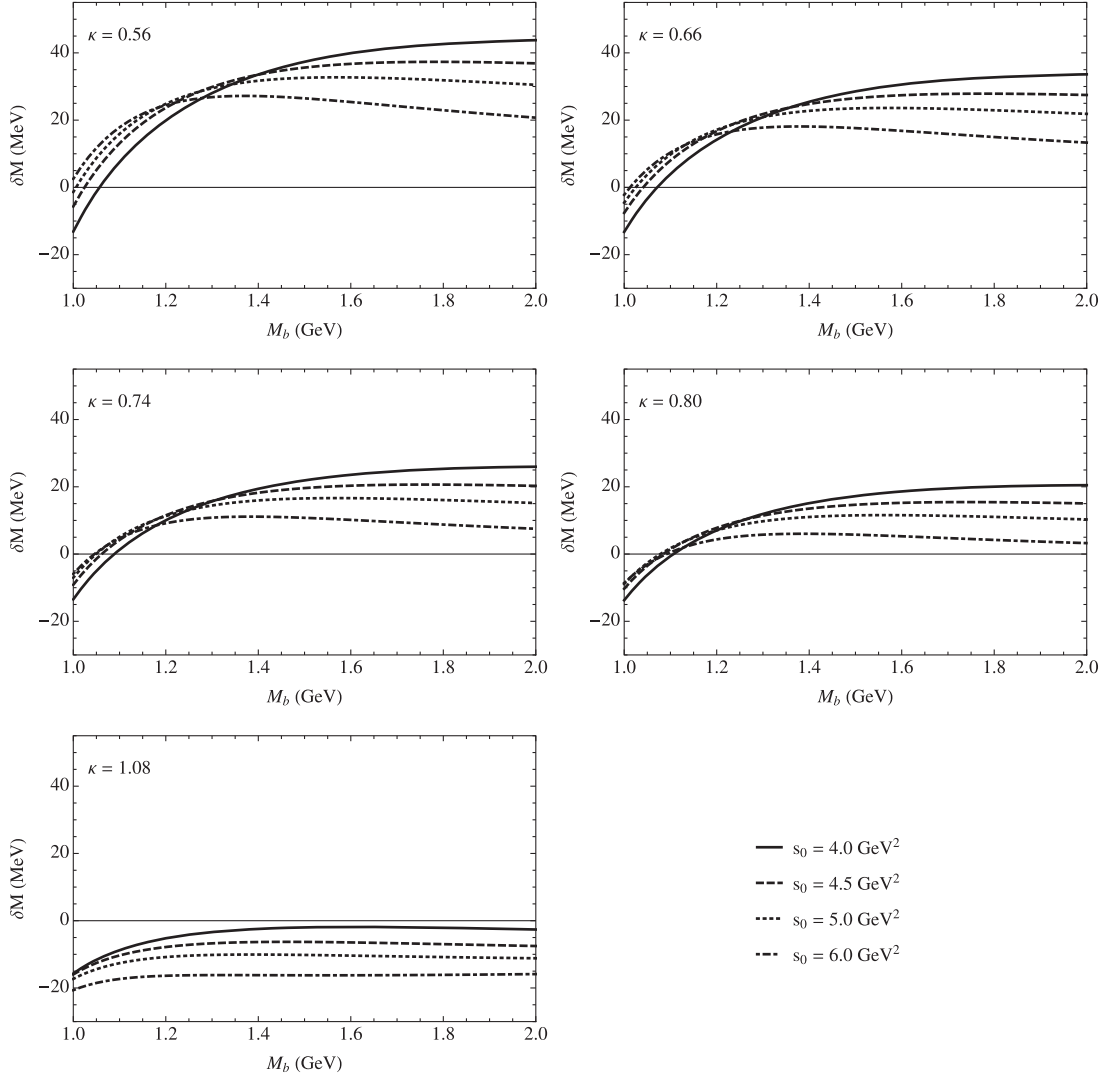
where

$$\tau = \frac{1}{M_b^2}, \quad (67)$$

and M_b is the Borel mass scale.

Extraction of the diquark mass prediction from (66) requires constraining the Borel window to the M_b region where the QCD prediction is reliable, and the methods used in Ref. [52] will be adopted. The first constraint limits the relative size of the continuum to control the uncertainties in the approximation (see, e.g., Refs. [43–45])

$$\frac{\mathcal{R}_1^{(\Gamma)}(\tau, s_0)/\mathcal{R}_0^{(\Gamma)}(\tau, s_0)}{\mathcal{L}_1^{(\Gamma)}(\tau)/\mathcal{L}_0^{(\Gamma)}(\tau)} \geq 0.5, \quad (68)$$

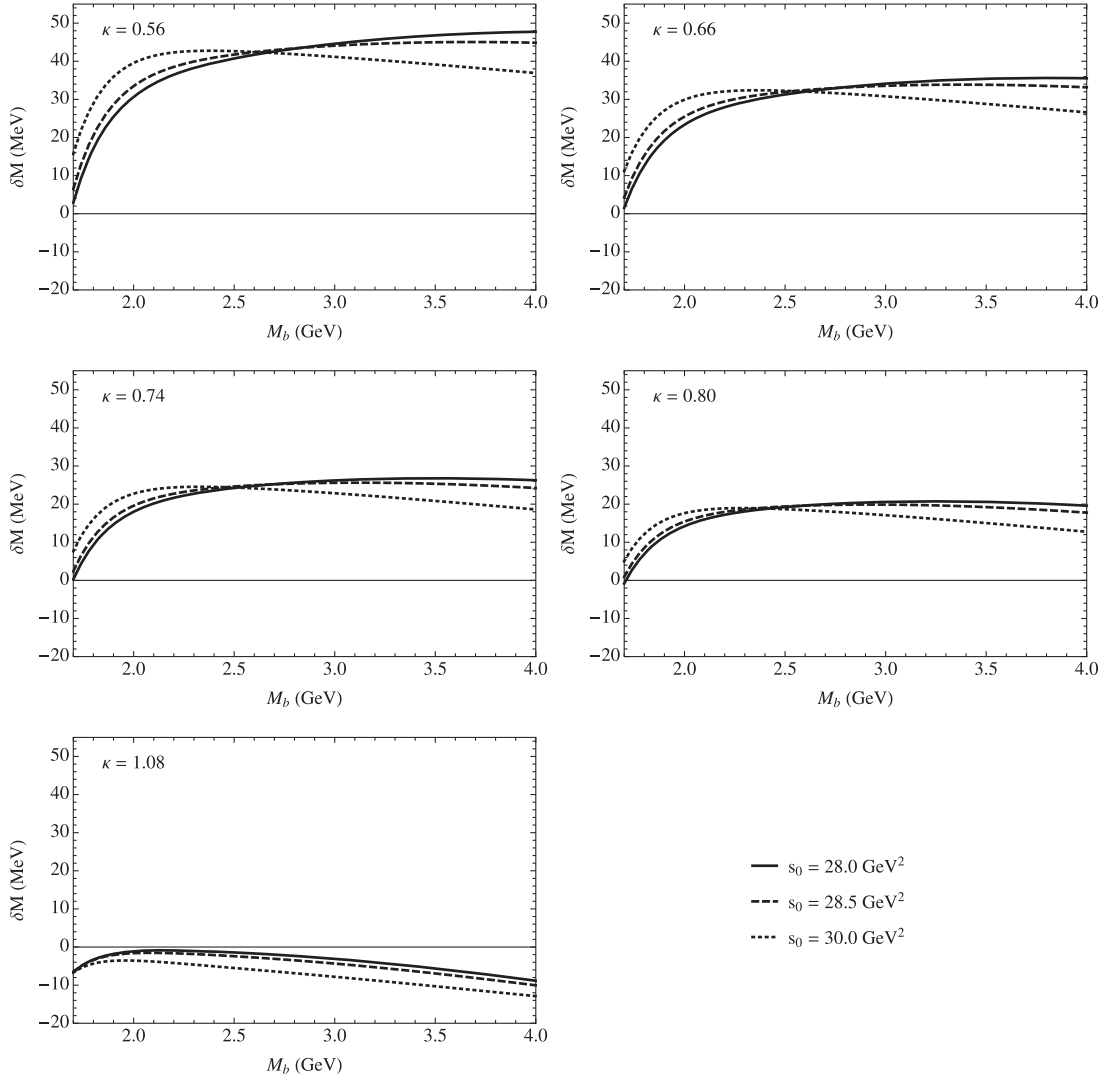which leads to an upper bound on M_b (lower bound on $\tau = 1/M_b^2$). Lower bounds on M_b are obtained via the

FIG. 13. The quantity $\delta M(M_b, s_0 + 2M_{[Qn]}\Delta)$ with $\Delta = 0$ as a function of M_b for $J^P = 0^+$ $[cq]$ diquarks with Table V κ values and selected s_0 near s_0^{opt} (see Table VI).

FIG. 14.   The quantity $\delta M(M_b, s_0 + 2M_{[Qn]}\Delta)$ with $\Delta = 0$ as a function of M_b for $J^P = 0^+$ $[bq]$ diquarks with Table V κ values and selected s_0 near s_0^{opt} (see Table VI).

Hoelder inequality technique of Ref. [114] which leads to the constraint[5]

$$\frac{\mathcal{R}_2^{(\Gamma)}(\tau, s_0)/\mathcal{R}_1^{(\Gamma)}(\tau, s_0)}{\mathcal{R}_1^{(\Gamma)}(\tau, s_0)/\mathcal{R}_0^{(\Gamma)}(\tau, s_0)} \geq 1. \qquad (69)$$

Because (69) is obtained by using positivity of the spectral function in (33), it represents the minimum requirement for the QCD prediction $\mathcal{R}_k^{(\Gamma)}(\tau, s_0)$ to be consistent with an integrated spectral function. The Borel window is thus the range of M_b where the sum rules satisfy the constraints of Eqs. (68) and (69). The minimum value for the continuum threshold s_0 can be

determined by requiring that the sum-rule ratio for the diquark mass ratio is stable under variations in the Borel scale (i.e., the sum-rule stability criterion)

$$\frac{d}{d\tau}M_\Gamma^2 = \frac{d}{d\tau}\left[\frac{\mathcal{R}_1^{(\Gamma)}(\tau, s_0)}{\mathcal{R}_0^{(\Gamma)}(\tau, s_0)}\right] = 0. \qquad (70)$$

Because the τ solution of (70) depends on s_0, the minimum value for the continuum threshold, $s_0^{\min}$, is the minimum value of s_0 for which the sum rule is stable inside the Borel window. If stability is achieved, then the predicted value of the diquark mass M_Γ and optimized value of s_0 is found by minimizing the following residual sum of squares

$$\chi_\Gamma^2(M_\Gamma, s_0) = \sum_{j=1}^{n}\left(\frac{1}{M_\Gamma}\sqrt{\frac{\mathcal{R}_1^{(\Gamma)}(\tau_j, s_0)}{\mathcal{R}_0^{(\Gamma)}(\tau_j, s_0)}} - 1\right)^2, \qquad (71)$$
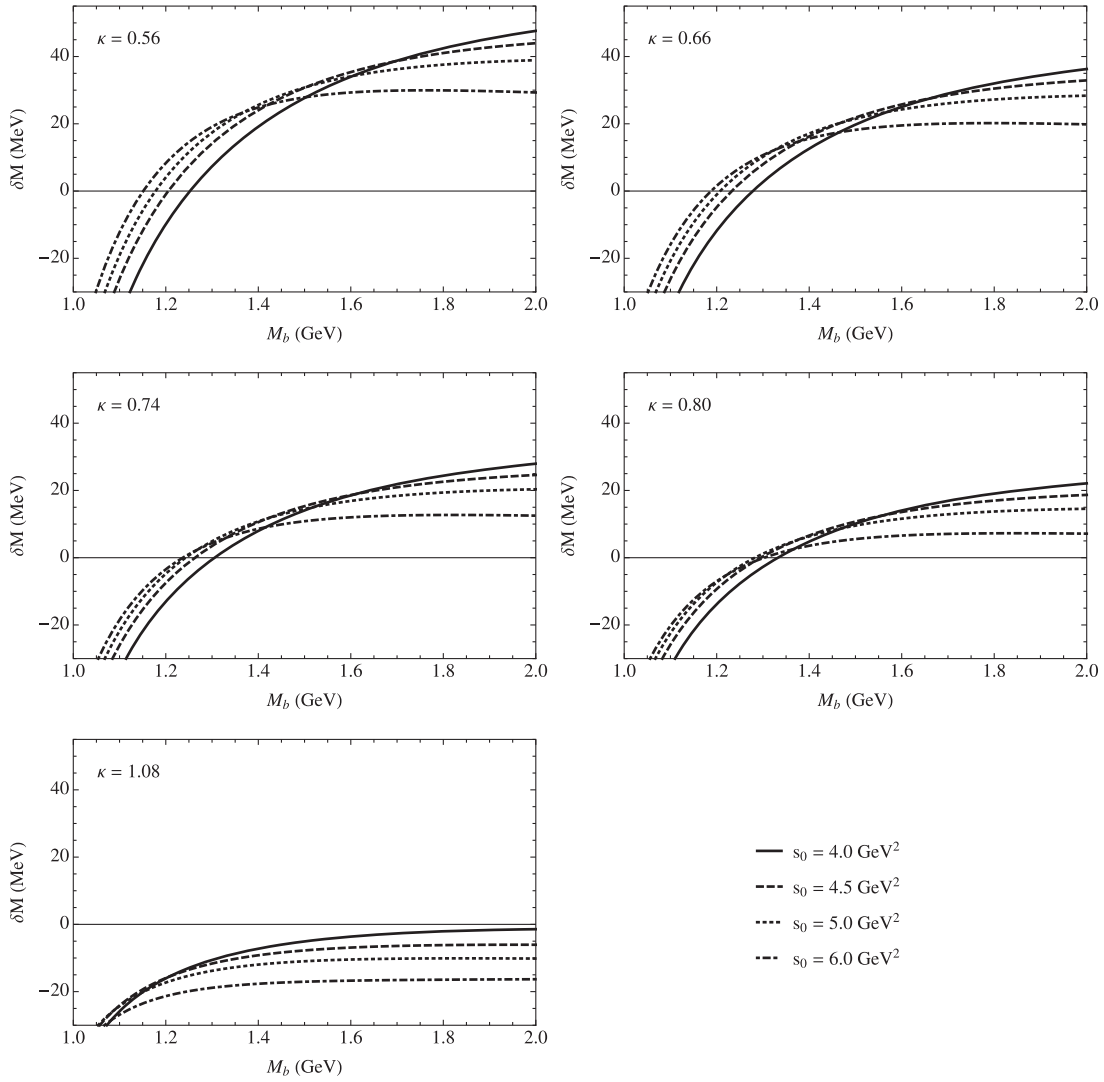
---

[5]As in Ref. [52], related constraints with higher-weight sum rules lead to less restrictive bounds than (69).

FIG. 15. The quantity $\delta M(M_b, s_0 + 2M_{[Qn]}\Delta)$ with $\Delta = 0$ as a function of M_b for $J^P = 1^+$ $[cq]$ diquarks with Table V κ values and selected s_0 near s_0^{opt} (see Table VI).

with respect to M_Γ and s_0, where the sum is over $n = 30$ equally spaced M_b points in the Borel window. The quantity M_Γ is implicitly a function of s_0 obtained by fitting (66) in the Borel window

$$M_\Gamma = \frac{1}{n}\sum_{j=1}^{n}\sqrt{\frac{\mathcal{R}_1^{(\Gamma)}(\tau_j, s_0)}{\mathcal{R}_0^{(\Gamma)}(\tau_j, s_0)}}, \qquad (72)$$

so minimization of (71) implicitly reduces to a one-dimensional optimization in s_0.

Using the above analysis methodology, the benchmark prediction of the heavy-nonstrange diquark mass $M_{[Qn]}$ is now performed. This analysis updates the previous determination of Ref. [52] by including the additional QCD condensate diagrams Figs. 8(b) and 9(b) and incorporating changes in the PDG quark mass parameters over the past

decade (in comparing the 2012 and 2022 PDG values of Refs. [93,115], the central values have changed and uncertainties have decreased). As in Ref. [52], the negative parity channels do not stabilize, and Fig. 11 shows the sum-rule ratio as a function of the Borel scale for various choices of s_0.[6] Figure 11 is almost indistinguishable from the corresponding figures in Ref. [52], and the resulting central values for $M_{[Qn]}$ shown in Table VI are slightly smaller than Ref. [52] but overlap within theoretical uncertainties.

Although the same procedure can be used to independently predict the $[Qs]$ diquark masses, the theoretical uncertainties in Table VI completely obscure the $M_{[Qs]} - M_{[Qn]}$ mass splitting. Inspired by the double-ratio

---

[6]The $s_0 \to \infty$ case provides a robust upper bound on the mass prediction, see, e.g., Ref. [83].

method which has been shown to reduce the theoretical uncertainty in $SU(3)$ flavor splittings [61], the following expression is used to determine the mass splitting δM using the $[Qn]$ analysis as a baseline

$$\delta M(M_b, s_0^{[Qs]}) \equiv \sqrt{\frac{\mathcal{R}_1^{[Qs]}(M_b, s_0^{[Qs]})}{\mathcal{R}_0^{[Qs]}(M_b, s_0^{[Qs]})}} - \sqrt{\frac{\mathcal{R}_1^{[Qn]}(M_b, s_0^{\text{opt}})}{\mathcal{R}_0^{[Qn]}(M_b, s_0^{\text{opt}})}},$$
(73)

where s_0^{opt} corresponds to the appropriate value in Table VI. Because Fig. 12 illustrates that the differences between strange and nonstrange Laplace sum-rules are small (particularly near s_0^{opt}), $s_0^{[Qs]} \approx s_0^{\text{opt}}$ and can be parametrized by the quantity Δ defined by

$$\Delta = M_{[Qs]} - M_{[Qn]} \ll M_{[Qn]},$$
(74)

$$s_0^{[Qs]} - s_0^{\text{opt}} = M_{[Qs]}^2 - M_{[Qn]}^2 \approx 2M_{[Qn]}\Delta,$$
(75)

where (75) is given to first-order in the small parameter $\Delta/M_{[Qn]} \ll 1$. A self-consistent solution for Δ of Eqs. (73)–(75) occurs when

$$\Delta = \delta M(M_b, s_0^{\text{opt}} + 2M_{[Qn]}\Delta).$$
(76)

Note that (76) is founded upon the $[Qn]$ sum-rule determinations $M_{[Qn]}$ and s_0^{opt} (see Table VI), quantities that are independent of the parameter κ. An iterative solution for (76) can be constructed via
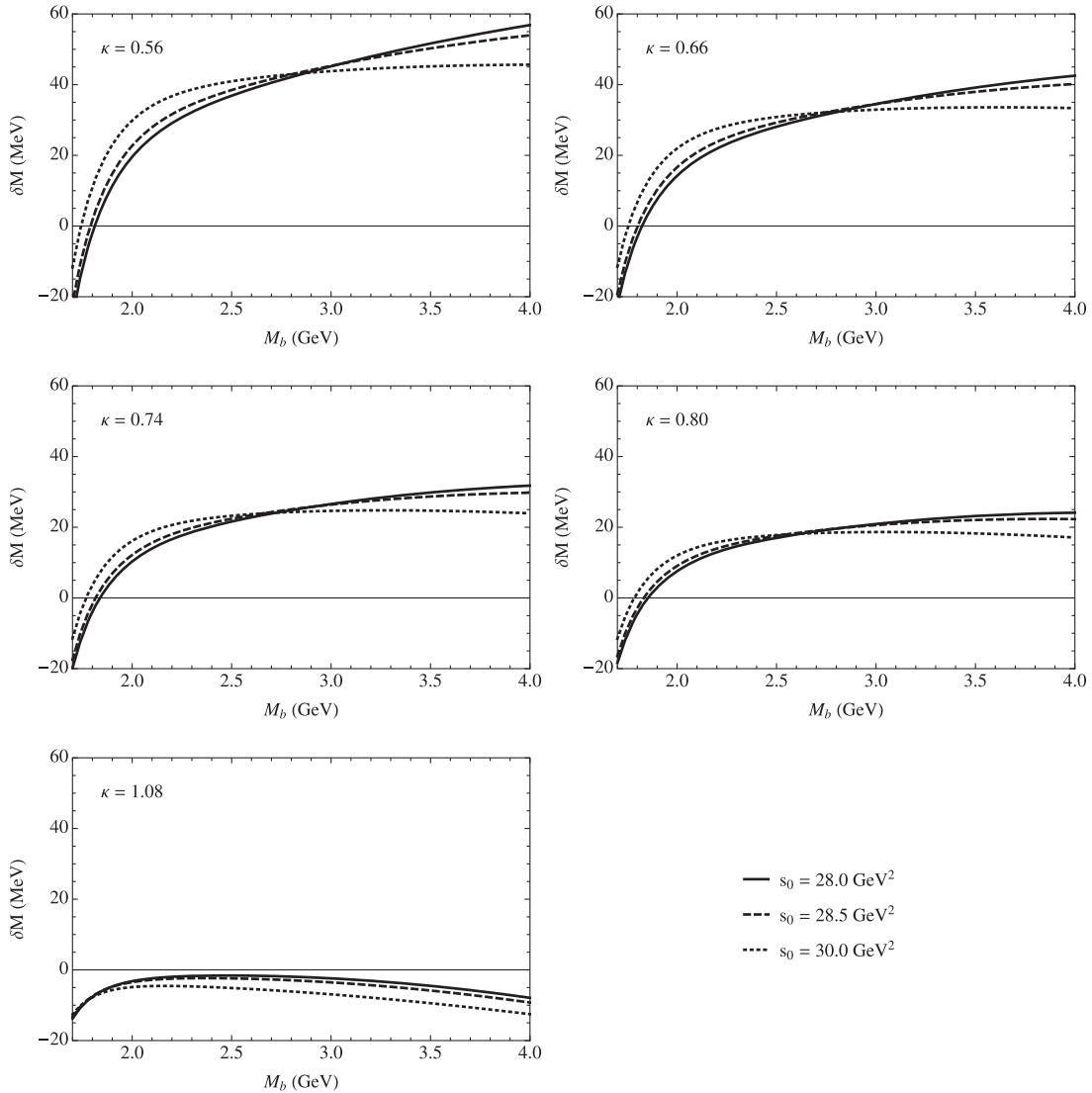

FIG. 16. The quantity $\delta M(M_b, s_0 + 2M_{[Qn]}\Delta)$ with $\Delta = 0$ as a function of M_b for $J^P = 1^+$ $[bq]$ diquarks with Table V κ values and selected s_0 near s_0^{opt} (see Table VI).
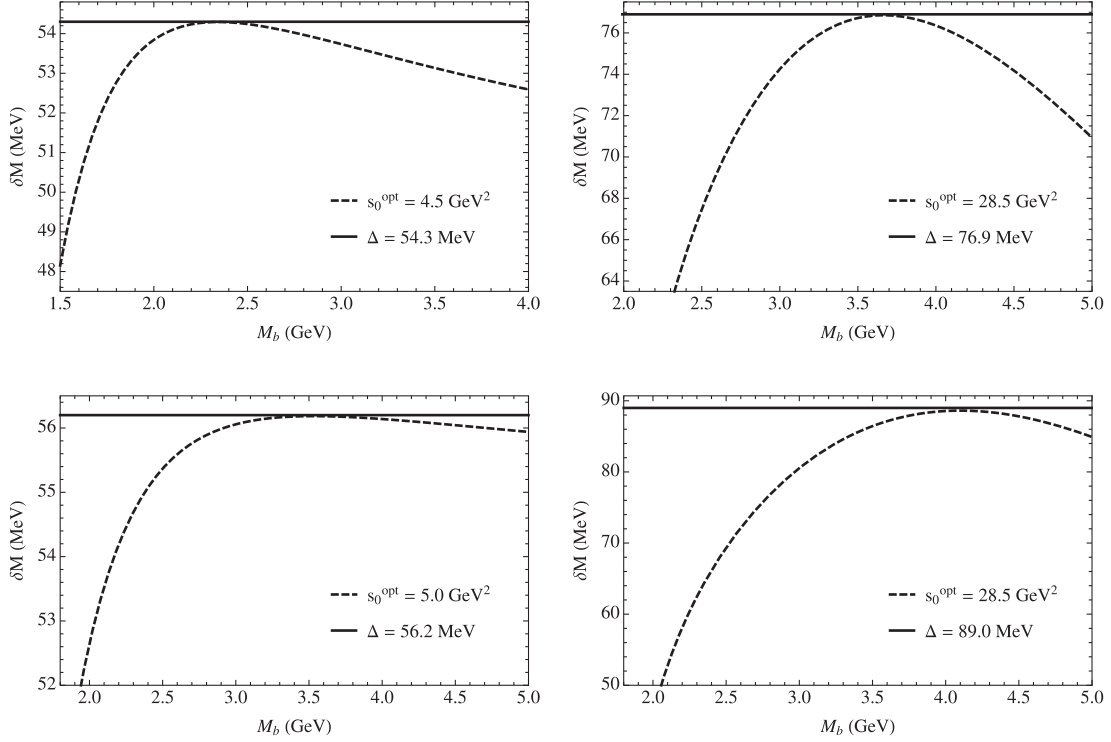
FIG. 17. The self-consistent solution of Eq. (76) for the mass splitting $\Delta = \delta M(M_b, s_0 + 2M_{[Qn]}\Delta)$ with $\kappa = 0.74$ is shown for 0^+ $[cq]$ diquarks (top left), 0^+ $[bq]$ diquarks (top right), 1^+ $[cq]$ diquarks (bottom left), and 1^+ $[bq]$ diquarks (bottom right).

$$\Delta_{n+1} = \delta M(M_b, s_0^{\mathrm{opt}} + 2M_{[Qn]}\Delta_n), \qquad (77)$$

with $\Delta_0 = 0$ to begin the iterative procedure. At each stage of the iteration, Δ_{n+1} is determined by the critical value (maximum) of δM defined by $\frac{d}{dM_b}\delta M = 0$ [i.e., the Eq. (70) stability criterion]. The initial step of the iteration is closely connected to the double-ratio method [61] because with $\Delta_0 = 0$ the continuum values in (31) are aligned and the double-ratio is then obtained by dividing (73) by $\sqrt{\mathcal{R}_1^{[Qn]}/\mathcal{R}_0^{[Qn]}}$. Figures 13–16 show this initial iterative step for selected values of κ and for s_0 values near s_0^{opt}. At this first iterative step, Figs. 13–16 show a general trend of decreasing mass splitting $\delta M = M_{[Qs]} - M_{[Qn]}$ as κ increases, and for the largest chosen κ the mass hierarchy inverts so that $M_{[Qs]} < M_{[Qn]}$.[7] The prominent role of κ in Figs. 13–16 reinforces the comment from Ref. [47] on the importance of improved determinations of κ.

It is clear that Figs. 13–16 do not represent a self-consistent solution of (76) for $\Delta = 0$ because $\delta M \neq 0$ at its critical (M_b stability) values. Thus, the final determination of the mass splitting $M_{[Qs]} - M_{[Qn]}$ is obtained from the self-consistent solution of (76), with upper and lower

bounds on $M_{[Qs]} - M_{[Qn]}$ resulting from $\kappa = 0.56$ chosen as the smallest sum-rule value from Ref. [46] and $\kappa = 0.74$ chosen from Ref. [102] as the most accurately determined sum-rule value (see, e.g., review in Ref. [105]).[8] The results for the self-consistent solution for the mass splitting $M_{[Qs]} - M_{[Qn]}$ are shown in Figs. 17–18 and summarized in Table VII. The maxima of δM used to construct the solution occur at M_b above the Borel window lower bound; the Borel window upper bound is not relevant in this analysis because δM suppresses the continuum contributions through the difference (73). Notice that the self-consistent solution increases the mass splitting $M_{[Qs]} - M_{[Qn]}$ compared to the initial iteration with $\Delta_0 = 0$ (see Figs. 13–16), so the limit $s_0^{[Qs]} = s_0^{[Qn]}$ provides a lower bound on $M_{[Qs]} - M_{[Qn]}$. Thus our final determination of the $J^P \in \{0^+, 1^+\}$ flavor splitting of diquark constituent masses is 55 MeV $\lesssim M_{[cs]} - M_{[cn]} \lesssim$ 100 MeV and 75 MeV $\lesssim M_{[bs]} - M_{[bn]} \lesssim$ 150 MeV, with a slight tendency for larger splittings for the $J^P = 1^+$ axial-vector channels.

Investigation of theoretical uncertainties in the mass splitting arising from QCD parameters shows that apart from κ all other effects are suppressed via the difference

---

[7]QCD sum-rule studies of tetraquarks have also found inverted mass hierarchies for larger κ [116].

[8]The central value $\kappa = 0.74$ of Ref. [102] is also consistent with the range $\kappa = 0.66 \pm 0.10$ of Ref. [46].
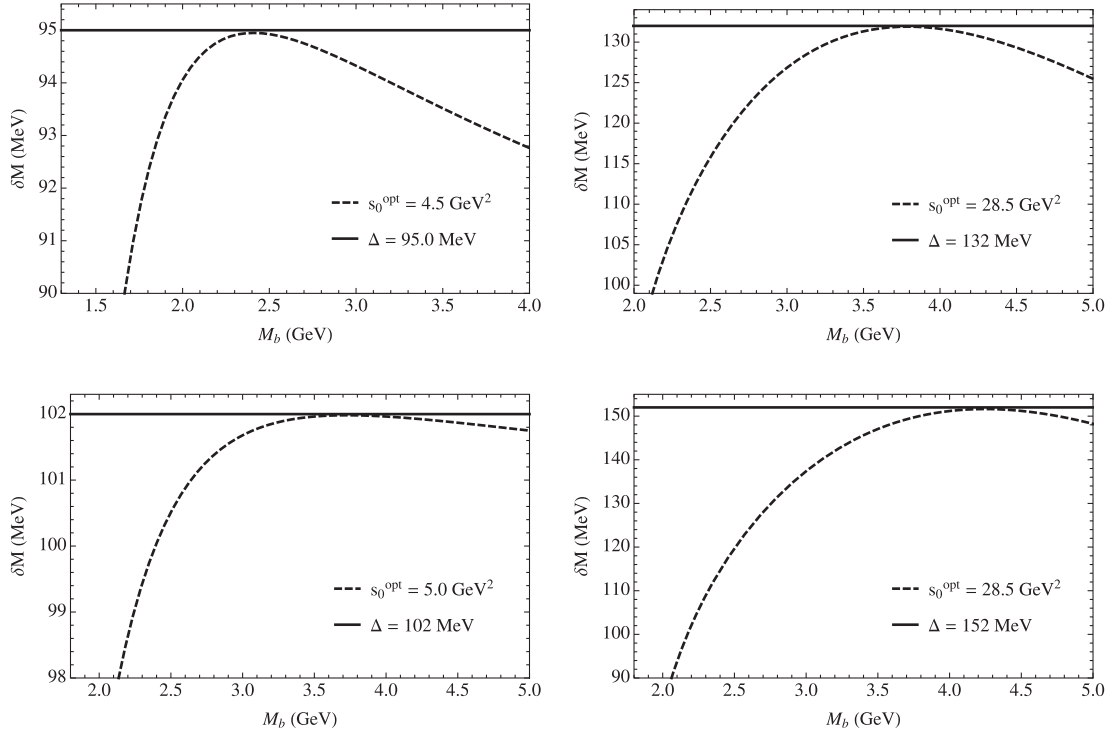
FIG. 18.   The self-consistent solution of Eq. (76) for the mass splitting $\Delta = \delta M(M_b, s_0 + 2M_{[Qn]}\Delta)$ with $\kappa = 0.56$ is shown for 0^+ $[cq]$ diquarks (top left), 0^+ $[bq]$ diquarks (top right), 1^+ $[cq]$ diquarks (bottom left), and 1^+ $[bq]$ diquarks (bottom right).

δM in Eq. (73), similar to the reduction in theoretical uncertainty in the double-ratio method [61]. Apart from the crucial parameter κ, which is specific to the strange channel and therefore cannot be suppressed in δM, the next most important quantity is r_{Qn} because of its appearance with κ in Eq. (54) for $m\langle \bar{s}s \rangle$. Variation of r_{Qn} over the range in Table V leads to ~5 MeV uncertainty in the Table VII mass splittings. Table VII also explores methodological uncertainty in the extraction of the mass splitting via the self-consistent solution for Δ using the critical value (maxima) in Figs. 17–18. This is done by comparing $M_{[Qs]}^{\Delta} = M_{[Qn]} + \Delta$ with the fitted value $M_{[Qs]}^{QCDSR}$ obtained via (72) for $s_0^{[Qs]}$ given by Eq. (75). As shown in Table VII, the resulting

methodological uncertainty is less than 5 MeV. Thus the theoretical uncertainty associated with κ is the dominant effect.

Finally, returning attention to $[ss]$ diquarks, the single-narrow-resonance analysis methodology discussed in detail below (64) can be applied in an attempt to predict a doubly strange diquark mass. However, substituting (42) and (43) into (66) leads to a monotonically decreasing function of τ for all reasonable values of s_0 as is illustrated in Fig. 19. Note that the τ interval used in Fig. 19, i.e., $\tau \leq 2$ GeV^{-2} suffices to cover the acceptable Borel window of any Laplace sum-rule analysis of light- or strange-quark systems. None of the plots have a local minimum, and so it can be concluded that the Laplace sum-rule analysis of $J^P = 1^+$ $[ss]$ diquarks fails to

TABLE VII.   The J^P diquark mass splittings $\Delta = M_{[Qs]} - M_{[Qn]}$ for selected κ obtained via the self-consistent solution of (76). The quantity $M_{[Qs]}^{\Delta}$ is the resulting diquark mass $M_{[Qs]}^{\Delta} = M_{[Qn]} + \Delta$ and $M_{[Qs]}^{QCDSR}$ is obtained by the fitted quantity (72) for s_0 given by Eq. (75).

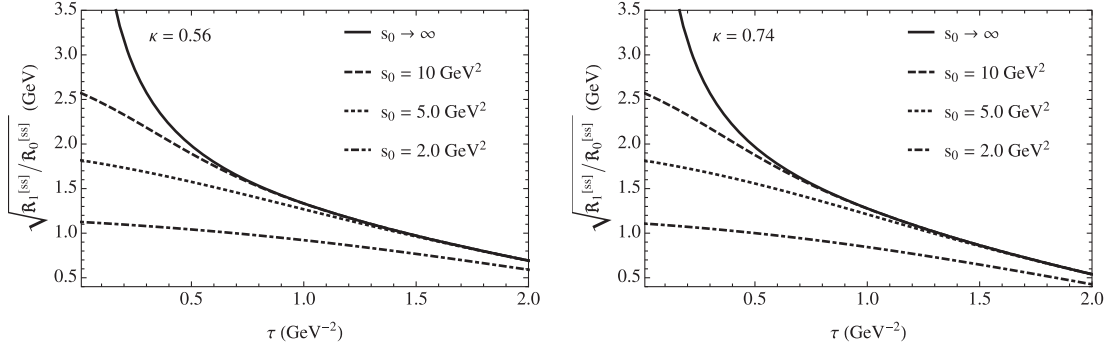| $[Qq]$	J^P	$\Delta = M_{[Qs]} - M_{[Qn]}$ (MeV)		$M_{[Qs]}^{\Delta}$ (GeV)		$M_{[Qs]}^{QCDSR}$ (GeV)	
		$\kappa = 0.74$	$\kappa = 0.56$	$\kappa = 0.74$	$\kappa = 0.56$	$\kappa = 0.74$	$\kappa = 0.56$
$[cq]$	0^+	54.3	95.0	1.83	1.87	1.82	1.85
	1^+	56.2	102	1.93	1.97	1.91	1.94
$[bq]$	0^+	76.9	132	5.05	5.10	5.04	5.09
	1^+	89.0	152	5.06	5.12	5.05	5.11

FIG. 19.   The quantity $\sqrt{\mathcal{R}_1^{[ss]}(\tau, s_0)/\mathcal{R}_0^{[ss]}(\tau, s_0)}$ for $J^P = 1^+$ [ss] diquarks with $\kappa = 0.56$ (left) and $\kappa = 0.74$ (right).

stabilize. This absence of sum-rule evidence for $J^P = 1^+$ [ss] diquarks is distinct from the stable sum-rule predictions for [cc] and [bb] axial-vector diquark constituent masses in Ref. [55].

IV. CONCLUSIONS

Motivated by the compact tetraquark diquark-antidiquark models for four-quark mesons, the constituent masses of $J^P \in \{0^+, 1^+\}$ heavy-light [Qq] and $J^P = 1^+$ [ss] diquarks have been studied in QCD Laplace sum rules. For the [Qq] diquarks, the sum-rule analysis focused on the $SU(3)$ flavor mass splittings. QCD correlation functions of $J^P \in \{0^\pm, 1^\pm\}$ [Qq] diquark composite operators were calculated up to NLO in perturbation theory, LO in the strange quark mass, and in the chiral limit for nonstrange (u, d) quarks with an isospin-symmetric vacuum $\langle \bar{n}n \rangle = \langle \bar{u}u \rangle = \langle \bar{d}d \rangle$. The $J^P = 1^+$ [ss] diquark correlation function was calculated up to NLO in perturbation theory and to order m_s^2 (i.e., the first nontrivial order) in the strange quark mass.

The challenges of diquark composite operator renormalization with inclusion of strange-quark masses were addressed by diagrammatic renormalization methods for QCD correlation functions [68]. These diagrammatic renormalization methods were validated by confirming the NLO chiral-limit perturbative results of Ref. [52].

Contrary to the stable sum-rule analysis of $J^P = 1^+$ [QQ] diquarks [55], the single-narrow-resonance Laplace sum-rule analysis of $J^P = 1^+$ [ss] diquark masses failed to stabilize. Consequently, no sum-rule evidence for the existence of $J^P = 1^+$ [ss] diquark states was discovered. Unlike the case for charm and bottom quarks, a physical interpretation of the unstable $J^P = 1^+$ [ss] sum-rule results is that the strange quark mass is insufficiently large to mitigate the effect of the spin-spin interaction (see, e.g., Ref. [20]) in a color-triplet S-wave diquark system. The lack of sum-rule evidence for [ss] diquarks can also guide interpretations for the internal structure of fully strange four-quark states. The Ref. [117] sum-rule analysis of fully strange four-quark states found similar stable mass predictions for both molecular and tetraquark currents, and thus the absence of evidence for [ss] diquarks favors the molecular interpretation of Ref. [117].

The QCD sum-rule methodology developed to reduce the theoretical uncertainty in the [Qq] diquark mass flavor splittings is inspired by the double-ratio method [61], and begins with a baseline prediction of the nonstrange constituent diquark masses $M_{[Qn]}$, updating Ref. [52] by inclusion of additional QCD condensate diagrams Figs. 8(b) and 9(b) and to reflect improved determinations of quark mass parameters. As in Ref. [52] negative parity $J^P \in \{0^-, 1^-\}$ sum-rule predictions do not stabilize, and the baseline $J^P \in \{0^+, 1^+\}M_{[Qn]}$ mass predictions agree with Ref. [52] within theoretical uncertainties, with slightly smaller central values.

The sum-rule methodology developed to calculate the diquark mass splittings $\Delta = M_{[Qs]} - M_{[Qn]}$ involves the self-consistent solution for Δ from Eq. (76). The strange quark condensate parameter $\kappa = \langle \bar{s}s \rangle / \langle \bar{n}n \rangle$ is found to have an important impact on $SU(3)$ flavor splittings, decreasing the mass difference $M_{[Qs]} - M_{[Qn]}$ as κ increases, and for sufficiently large κ the mass hierarchy inverts to give $M_{[Qs]} < M_{[Qn]}$. In the typical QCD sum-rule range $0.56 < \kappa < 0.74$, the final determination of the $J^P \in \{0^+, 1^+\}$ flavor splitting of diquark constituent masses is (see Table VII)

$$55 \text{ MeV} \lesssim M_{[cs]} - M_{[cn]} \lesssim 100 \text{ MeV},$$
$$75 \text{ MeV} \lesssim M_{[bs]} - M_{[bn]} \lesssim 150 \text{ MeV}, \tag{78}$$

with a slight tendency for larger splittings for the $J^P = 1^+$ axial-vector channels. Other sources of theoretical uncertainty in $M_{[Qs]} < M_{[Qn]}$ were found to be smaller than ~ 5 MeV.

In comparison to the constituent diquark mass parameters used in models of tetraquarks (and pentaquarks), the QCD sum-rule predictions $M_{[Qs]} - M_{[Qn]}$ obtained in this work are in good agreement with the $M_{[Qs]} - M_{[Qn]} \approx 100$ MeV values in the dynamical quark model [28] and relativistic quark model [34–38]. However, the

$M_{[Qs]} - M_{[Qn]} \approx 200$ MeV values used in type I/II diquark models [22–27] and in the diquark effective Hamiltonian model [39] are somewhat larger than our QCD sum-rule predictions. The relativized diquark model [29–33] has quite different patterns of mass splitting, with $M_{[bs]} - M_{[bn]} \ll M_{[cs]} - M_{[cn]}$, whereas our sum-rule predictions have $M_{[bs]} - M_{[bn]} \approx M_{[cs]} - M_{[cn]}$. In conclusion, the QCD sum-rule predictions of the $M_{[Qs]} - M_{[Qn]}$ mass splittings in Eq. (78) provide good supporting QCD evidence for the diquark constituent mass parameters used in the dynamical quark model [28] and relativistic quark model [34–38].

[1] E. S. Swanson, Phys. Rep. **429**, 243 (2006).
[2] S. Godfrey and S. L. Olsen, Annu. Rev. Nucl. Part. Sci. **58**, 51 (2008).
[3] H.-X. Chen, W. Chen, X. Liu, and S.-L. Zhu, Phys. Rep. **639**, 1 (2016).
[4] R. F. Lebed, R. E. Mitchell, and E. S. Swanson, Prog. Part. Nucl. Phys. **93**, 143 (2017).
[5] A. Ali, J. S. Lange, and S. Stone, Prog. Part. Nucl. Phys. **97**, 123 (2017).
[6] S. L. Olsen, T. Skwarnicki, and D. Zieminska, Rev. Mod. Phys. **90**, 015003 (2018).
[7] N. Brambilla, S. Eidelman, C. Hanhart, A. Nefediev, C.-P. Shen, C. E. Thomas, A. Vairo, and C.-Z. Yuan, Phys. Rep. **873**, 1 (2020).
[8] Y.-R. Liu, H.-X. Chen, W. Chen, X. Liu, and S.-L. Zhu, Prog. Part. Nucl. Phys. **107**, 237 (2019).
[9] H.-X. Chen, W. Chen, X. Liu, Y.-R. Liu, and S.-L. Zhu, Rep. Prog. Phys. **86**, 026201 (2023).
[10] R. L. Jaffe, Phys. Rev. D **15**, 267 (1977).
[11] R. L. Jaffe, Phys. Rev. D **15**, 281 (1977).
[12] R. Aaij *et al.* (LHCb Collaboration), Phys. Rev. Lett. **131**, 041902 (2023).
[13] R. Aaij *et al.* (LHCb Collaboration), Phys. Rev. D **108**, 012017 (2023).
[14] T. Gershon (LHCb Collaboration), arXiv:2206.15233.
[15] R. Aaij *et al.* (LHCb Collaboration), Sci. Bull. **65**, 1983 (2020).
[16] R. Aaij *et al.* (LHCb Collaboration), Phys. Rev. Lett. **125**, 242001 (2020).
[17] R. Aaij *et al.* (LHCb Collaboration), Phys. Rev. D **102**, 112003 (2020).
[18] M. Ablikim *et al.* (BESIII Collaboration), Phys. Rev. Lett. **126**, 102001 (2021).
[19] R. Aaij *et al.* (LHCb Collaboration), Phys. Rev. Lett. **127**, 082001 (2021).
[20] R. L. Jaffe, Phys. Rep. **409**, 1 (2005).
[21] M. Anselmino, E. Predazzi, S. Ekelin, S. Fredriksson, and D. B. Lichtenberg, Rev. Mod. Phys. **65**, 1199 (1993).
[22] L. Maiani, F. Piccinini, A. D. Polosa, and V. Riquer, Phys. Rev. D **71**, 014028 (2005).
[23] L. Maiani, V. Riquer, F. Piccinini, and A. D. Polosa, Phys. Rev. D **72**, 031502 (2005).
[24] L. Maiani, V. Riquer, R. Faccini, F. Piccinini, A. Pilloni, and A. D. Polosa, Phys. Rev. D **87**, 111102 (2013).
[25] R. F. Lebed and A. D. Polosa, Phys. Rev. D **93**, 094024 (2016).
[26] L. Maiani, A. D. Polosa, and V. Riquer, Sci. Bull. **66**, 1616 (2021).
[27] L. Maiani, F. Piccinini, A. D. Polosa, and V. Riquer, Phys. Rev. D **89**, 114010 (2014).
[28] J. F. Giron, R. F. Lebed, and S. R. Martinez, Phys. Rev. D **104**, 054001 (2021).
[29] M. N. Anwar, J. Ferretti, and E. Santopinto, Phys. Rev. D **98**, 094015 (2018).
[30] J. Ferretti and E. Santopinto, J. High Energy Phys. 04 (2020) 119.
[31] M. A. Bedolla, J. Ferretti, C. D. Roberts, and E. Santopinto, Eur. Phys. J. C **80**, 1004 (2020).
[32] M. N. Anwar, J. Ferretti, F.-K. Guo, E. Santopinto, and B.-S. Zou, Eur. Phys. J. C **78**, 647 (2018).
[33] J. Ferretti, Few Body Syst. **60**, 17 (2019).
[34] D. Ebert, R. N. Faustov, and V. O. Galkin, Phys. Lett. B **634**, 214 (2006).
[35] D. Ebert, R. N. Faustov, V. O. Galkin, and W. Lucha, Phys. Rev. D **76**, 114015 (2007).
[36] D. Ebert, R. N. Faustov, and V. O. Galkin, Eur. Phys. J. C **58**, 399 (2008).
[37] D. Ebert, R. N. Faustov, and V. O. Galkin, Phys. Lett. B **696**, 241 (2011).
[38] R. N. Faustov, V. O. Galkin, and E. M. Savchenko, Universe **7**, 94 (2021).
[39] P.-P. Shi, F. Huang, and W.-L. Wang, Phys. Rev. D **103**, 094038 (2021).
[40] P.-P. Shi, F. Huang, and W.-L. Wang, Eur. Phys. J. A **57**, 237 (2021).
[41] R. Zhu and C.-F. Qiao, Phys. Lett. B **756**, 259 (2016).
[42] J. F. Giron and R. F. Lebed, Phys. Rev. D **104**, 114028 (2021).
[43] M. A. Shifman, A. I. Vainshtein, and V. I. Zakharov, Nucl. Phys. **B147**, 385 (1979).
[44] M. A. Shifman, A. I. Vainshtein, and V. I. Zakharov, Nucl. Phys. **B147**, 448 (1979).
[45] L. J. Reinders, H. Rubinstein, and S. Yazaki, Phys. Rep. **127**, 1 (1985).

[46] S. Narison, *QCD as a Theory of Hadrons: From Partons to Confinement* (Oxford University Press, New York, 2005), Vol. 17.

[47] P. Gubler and D. Satow, Prog. Part. Nucl. Phys. **106**, 1 (2019).

[48] P. Colangelo and A. Khodjamirian, in *At The Frontier of Particle Physics*, edited by M. Shifman and B. Ioffe (World Scientific, Singapore, 2000), pp. 1495–1576.

[49] H. G. Dosch, M. Jamin, and B. Stech, Z. Phys. C **42**, 167 (1989).

[50] M. Jamin and M. Neubert, Phys. Lett. B **238**, 387 (1990).

[51] A. Zhang, T. Huang, and T. G. Steele, Phys. Rev. D **76**, 036004 (2007).

[52] R. T. Kleiv, T. G. Steele, A. Zhang, and I. Blokland, Phys. Rev. D **87**, 125018 (2013).

[53] Z.-G. Wang, Commun. Theor. Phys. **59**, 451 (2013).

[54] Z.-G. Wang, Eur. Phys. J. C **71**, 1524 (2011).

[55] S. Esau, A. Palameta, R. T. Kleiv, D. Harnett, and T. G. Steele, Phys. Rev. D **100**, 074025 (2019).

[56] J. Ho, R. Berg, W. Chen, D. Harnett, and T. G. Steele, Phys. Rev. D **98**, 096020 (2018).

[57] J. Ho, D. Harnett, and T. G. Steele, Nucl. Part. Phys. Proc. **294**–**296**, 75 (2018).

[58] J. Ho, D. Harnett, and T. G. Steele, J. High Energy Phys. 05 (2017) 149.

[59] W. Chen, H.-X. Chen, X. Liu, T. G. Steele, and S.-L. Zhu, Phys. Rev. D **96**, 114017 (2017).

[60] W. Chen, H.-X. Chen, X. Liu, T. G. Steele, and S.-L. Zhu, Phys. Rev. D **95**, 114005 (2017).

[61] S. Narison, Phys. Lett. B **210**, 238 (1988).

[62] E. Bagan, M. R. Ahmady, V. Elias, and T. G. Steele, Z. Phys. C **61**, 157 (1994).

[63] R. T. Kleiv and T. G. Steele, J. Phys. G **38**, 025001 (2011); **39**, 039501(E) (2012).

[64] K. Hepp, Commun. Math. Phys. **2**, 301 (1966).

[65] W. Zimmermann, Commun. Math. Phys. **15**, 208 (1969).

[66] J. C. Collins, *Renormalization*, Cambridge Monographs on Mathematical Physics Vol. 26 (Cambridge University Press, Cambridge, England, 1986).

[67] N. N. Bogoliubov and D. V. Shirkov, *Introduction to the Theory of Quantized Fields* (Wiley, New York, 1980).

[68] T. de Oliveira, D. Harnett, A. Palameta, and T. G. Steele, Phys. Rev. D **106**, 114023 (2022).

[69] R. Mertig, M. Bohm, and A. Denner, Comput. Phys. Commun. **64**, 345 (1991).

[70] V. Shtabovenko, R. Mertig, and F. Orellana, Comput. Phys. Commun. **207**, 432 (2016).

[71] V. Shtabovenko, R. Mertig, and F. Orellana, Comput. Phys. Commun. **256**, 107478 (2020).

[72] R. Mertig and R. Scharf, Comput. Phys. Commun. **111**, 265 (1998).

[73] O. V. Tarasov, Phys. Rev. D **54**, 6479 (1996).

[74] O. V. Tarasov, Nucl. Phys. **B502**, 455 (1997).

[75] H. H. Patel, Comput. Phys. Commun. **197**, 276 (2015).

[76] H. H. Patel, Comput. Phys. Commun. **218**, 66 (2017).

[77] E. E. Boos and A. I. Davydychev, Theor. Math. Phys. **89**, 1052 (1991).

[78] A. I. Davydychev, J. Math. Phys. (N.Y.) **33**, 358 (1992).

[79] D. J. Broadhurst, J. Fleischer, and O. V. Tarasov, Z. Phys. C **60**, 287 (1993).

[80] T. Huber and D. Maitre, Comput. Phys. Commun. **175**, 122 (2006).

[81] T. Huber and D. Maitre, Comput. Phys. Commun. **178**, 755 (2008).

[82] D. Maitre, Comput. Phys. Commun. **174**, 222 (2006).

[83] D. Harnett, T. G. Steele, and V. Elias, Nucl. Phys. **A686**, 393 (2001).

[84] L. Lewin, *Polylogarithms and Associated Functions* (North-Holland, Amsterdam, 1981).

[85] R. Kleiv, QCD sum rule studies of heavy quarkonium-like states, Ph.D. thesis, Saskatchewan University, 2013, arXiv: 1407.2292.

[86] S. Narison, N. Pak, and N. Paver, Phys. Lett. B **147**, 162 (1984).

[87] D. Harnett, R. T. Kleiv, K. Moats, and T. G. Steele, Nucl. Phys. **A850**, 110 (2011).

[88] E. Bagan, J. I. Latorre, and P. Pascual, Z. Phys. C **32**, 43 (1986).

[89] M. Jamin and M. Munz, Z. Phys. C **60**, 569 (1993).

[90] R. A. Bertlmann, G. Launer, and E. de Rafael, Nucl. Phys. **B250**, 61 (1985).

[91] P. Pascual and R. Tarrach, *QCD: Renormalization for the Practitioner* (Springer, New York, 1984), Vol. 194.

[92] P. A. Zyla *et al.* (Particle Data Group), Prog. Theor. Exp. Phys. **2020**, 083C01 (2020).

[93] R. L. Workman *et al.* (Particle Data Group), Prog. Theor. Exp. Phys. **2022**, 083C01 (2022).

[94] S. Narison, Phys. Lett. B **707**, 259 (2012).

[95] M. Gell-Mann, R. J. Oakes, and B. Renner, Phys. Rev. **175**, 2195 (1968).

[96] C. A. Dominguez and M. Loewe, Phys. Rev. D **31**, 2930 (1985).

[97] S. Narison, Phys. Lett. B **358**, 113 (1995).

[98] C. A. Dominguez, A. Ramlakan, and K. Schilcher, Phys. Lett. B **511**, 59 (2001).

[99] C. A. Dominguez, N. F. Nasrallah, and K. Schilcher, J. High Energy Phys. 02 (2008) 072.

[100] B. L. Ioffe, Nucl. Phys. **B188**, 317 (1981); **B191**, 591(E) (1981).

[101] L. J. Reinders, H. R. Rubinstein, and S. Yazaki, Phys. Lett. **120B**, 209 (1983); **122B**, 487(E) (1983).

[102] R. M. Albuquerque, S. Narison, and M. Nielsen, Phys. Lett. B **684**, 236 (2010).

[103] C. McNeile, A. Bazavov, C. T. H. Davies, R. J. Dowdall, K. Hornbostel, G. P. Lepage, and H. D. Trottier, Phys. Rev. D **87**, 034503 (2013).

[104] M. Jamin, Phys. Lett. B **538**, 71 (2002).

[105] D. Harnett, J. Ho, and T. G. Steele, Phys. Rev. D **103**, 114005 (2021).

[106] H. Dosch, M. Jamin, and S. Narison, Phys. Lett. B **220**, 251 (1989).

[107] S. Narison, Phys. Lett. B **626**, 101 (2005).

[108] S. Narison, Phys. Lett. B **718**, 1321 (2013).

[109] N. Gray, D. J. Broadhurst, W. Grafe, and K. Schilcher, Z. Phys. C **48**, 673 (1990).

[110] D. Broadhurst, N. Gray, and K. Schilcher, Z. Phys. C **52**, 111 (1991).

[111] J. Fleischer, F. Jegerlehner, O. Tarasov, and O. Veretin, Nucl. Phys. **B539**, 671 (1999).

[112] K. Chetyrkin and M. Steinhauser, Nucl. Phys. **B573**, 617 (2000).

[113] S. Narison and E. de Rafael, Phys. Lett. **103B**, 57 (1981).

[114] M. Benmerrouche, G. Orlandini, and T. G. Steele, Phys. Lett. B **356**, 573 (1995).

[115] J. Beringer *et al.* (Particle Data Group), Phys. Rev. D **86**, 010001 (2012).

[116] R. D. Matheus, S. Narison, M. Nielsen, and J. M. Richard, Phys. Rev. D **75**, 014005 (2007).

[117] H.-Z. Xi, Y.-W. Jiang, H.-X. Chen, A. Hosaka, and N. Su, arXiv:2307.07819.